THE JOURNAL OF BIOLOGICAL CHEMISTRY VOL. 290, NO. 39, pp. 23692–23710, September 25, 2015

L-type Calcium Channel $Ca_v1.2$ Is Required for Maintenance of Auditory Brainstem Nuclei*

Received for publication, June 15, 2015, and in revised form, July 30, 2015 Published, JBC Papers in Press, August 4, 2015, DOI 10.1074/jbc.M115.672675

Lena Ebbers[‡], Somisetty V. Satheesh[‡], Katrin Janz[§], Lukas Rüttiger[¶], Maren Blosa[‖], Franz Hofmann[**], Markus Morawski[‖], Désirée Griesemer[§], Marlies Knipper[¶], Eckhard Friauf[§], and Hans Gerd Nothwang[‡ ‡‡1]

From the [‡]Neurogenetics Group, Center of Excellence Hearing4All, School of Medicine and Health Sciences, Carl von Ossietzky University Oldenburg, 26111 Oldenburg, Germany, the [§]Animal Physiology Group, Department of Biology, University of Kaiserlautern, P. O. Box 3049, 67663 Kaiserslautern, Germany, the [¶]Department of Otolaryngology, Hearing Research Centre Tübingen (THRC), Molecular Physiology of Hearing, University of Tübingen, Elfriede Aulhorn Strasse 5, 72076 Tübingen, Germany, the [‖]Paul Flechsig Institute of Brain Research, Faculty of Medicine, University Leipzig, Liebigstrasse 19, 04103 Leipzig, Germany, the [**]Institut für Pharmakologie und Toxikologie, Technische Universität, Biedersteiner Strasse 29, D-80802 München, and the [‡‡]Research Center for Neurosensory Science, Carl von Ossietzky University Oldenburg, 26111 Oldenburg, Germany

Background: $Ca_v1.2$ is a calcium channel involved in excitation-coupled postsynaptic signaling.
Results: Targeted deletion of $Ca_v1.2$ in the auditory brainstem causes early postnatal cell death.
Conclusion: $Ca_v1.2$ is essential for the survival of auditory brainstem neurons shortly after circuit formation.
Significance: This study identifies the common and distinct functions of neuronal L-type calcium channels.

$Ca_v1.2$ and $Ca_v1.3$ are the major L-type voltage-gated Ca^{2+} channels in the CNS. Yet, their individual *in vivo* functions are largely unknown. Both channel subunits are expressed in the auditory brainstem, where $Ca_v1.3$ is essential for proper maturation. Here, we investigated the role of $Ca_v1.2$ by targeted deletion in the mouse embryonic auditory brainstem. Similar to $Ca_v1.3$, loss of $Ca_v1.2$ resulted in a significant decrease in the volume and cell number of auditory nuclei. Contrary to the deletion of $Ca_v1.3$, the action potentials of lateral superior olive (LSO) neurons were narrower compared with controls, whereas the firing behavior and neurotransmission appeared unchanged. Furthermore, auditory brainstem responses were nearly normal in mice lacking $Ca_v1.2$. Perineuronal nets were also unaffected. The medial nucleus of the trapezoid body underwent a rapid cell loss between postnatal days P0 and P4, shortly after circuit formation. Phosphorylated cAMP response element-binding protein (CREB), nuclear NFATc4, and the expression levels of p75NTR, Fas, and FasL did not correlate with cell death. These data demonstrate for the first time that both $Ca_v1.2$ and $Ca_v1.3$ are necessary for neuronal survival but are differentially required for the biophysical properties of neurons. Thus, they perform common as well as distinct functions in the same tissue.

L-type voltage-gated Ca^{2+} channels (L-VGCCs)[2] serve as key transducers in the plasma membrane, converting membrane depolarization to intracellular signaling (1). They consist of a pore-forming $\alpha1$ subunit and auxiliary $\alpha2$, β, γ, and δ subunits (1, 2). Of the four $\alpha1$ subunits, $Ca_v1.1$–$Ca_v1.4$, neurons mainly express $Ca_v1.2$ and $Ca_v1.3$ (3). During brain development, these two subunits participate in various processes such as neuronal survival (4, 5), neurite outgrowth (6, 7), the maturation of GABAergic synapses (8, 9), the positioning of the axon initiation segment (10), and myelination (11). In the mature brain, L-VGCCs are important for long-term potentiation (12) and glutamate receptor trafficking (13, 14).

The lack of isoform-specific pharmacological tools against the two subunits has long precluded the dissection of their precise *in vivo* roles (15, 16). Results from human genetics and transgenic mice have only recently provided some insights into these roles (16). In humans, mutations in *Cacna1c*, which encodes $Ca_v1.2$, are associated with Timothy syndrome, characterized by cardiac arrhythmia, syndactyly, cognitive abnormalities, and autism (17), Brugada syndrome-3 (18), associated with shorter QT intervals or early repolarization syndrome with an abnormal electroencephalography pattern (19). Furthermore, genome-wide association studies have linked *Cacna1c* polymorphisms to psychiatric disorders such as schizophrenia and bipolar disorders (20–22). In mice, constitutive ablation of *Cacna1c* causes embryonic lethality (23), whereas region-specific deletion in the hippocampus and neocortex

* This work was supported by Grants 428/10-1, Fri1784/15-1, and Mo2249/2-1 from the Deutsche Forschungsgemeinschaft (DFG), priority program 1608, "Ultrafast and Temporally Precise Information Processing: Normal and Dysfunctional Hearing"; CAVNET Grant MRTN-CT-2006-035367 (to H. G. N.) from the European Union; and a grant from the Cluster of Excellence Hearing4All (to H. G. N.). The authors declare that they have no conflicts of interest with the contents of this article.
[1] To whom correspondence should be addressed: Dept. of Neurogenetics, Center of Excellence Hearing4All, Carl von Ossietzky University, 26111 Oldenburg, Germany. Tel.: 49-441-798-3932; Fax: 49-441-798-5649; E-mail: hans.g.nothwang@uni-oldenburg.de.
[2] The abbreviations used are: L-VGCC, L-type voltage-gated Ca^{2+} channel; P, postnatal day (*e.g.* P0, P25); VGlut1, vesicular glutamate transporter; p-CREB, phosphorylated cAMP response element-binding protein; NFATc4, nuclear factor of activated T-cells, cytoplasmic 4; p75NTR, p75 neurotrophin receptor; Sort1, sortilin 1; Iba1, ionized calcium-binding adapter molecule 1; NeuN, neuronal nuclei; Kcnma1, potassium large conductance calcium-activated channel, subfamily M, α member 1; LSO, lateral superior olive; SOC, superior olivary complex; RPL3, ribosomal protein 3; FasL, Fas ligand; ABR, auditory brainstem response; DPOAE, distortion product otoacoustic emission; CNC, cochlear nucleus complex; AVCN, anterior ventral cochlear nucleus; PVCN, posterior ventral cochlear nucleus; DCN, dorsal cochlear nucleus; MNTB, medial nucleus of the trapezoid body; PN, perineuronal net; SPL, sound pressure level; eIPSC, evoked inhibitory postsynaptic current; mEPSC, miniature excitatory postsynaptic current; mIPSC, miniature inhibitory postsynaptic current.

results in impaired spatial learning (24). Conversely, the altered function of $Ca_v1.3$ is linked to sinoatrial node dysfunction and deafness (25, 26), impaired consolidation of fear memory (27), autism spectrum disorders (28), and adrenal aldosterone-producing adenomas (29). However, virtually nothing is known about the individual roles of $Ca_v1.2$ and $Ca_v1.3$ during neuronal development, despite the fact that numerous pharmacological studies have demonstrated the importance of L-VGCCs for neuronal survival *in vitro* and *in vivo* (5, 30–32).

We recently reported an essential role of $Ca_v1.3$ in the proper development and function of auditory brainstem structures in mice; the lack of $Ca_v1.3$ channels results in a reduced volume of major auditory nuclei (33, 34), impaired refinement of tonotopic projections (35), and abnormal auditory brainstem responses (34). Auditory brainstem neurons express both $Ca_v1.2$ and $Ca_v1.3$ (36). Therefore, they offer an excellent opportunity to delineate the contributions of both channels to neuronal development and function. To investigate the role of $Ca_v1.2$, here we employed a conditional knock-out approach and deleted *Cacna1c* in the mouse auditory brainstem from the embryonic stages onward. This resulted in structural abnormalities of the auditory nuclei. In contrast to the scenario following $Ca_v1.3$ loss, auditory brainstem responses were nearly normal. Perinatal analyses revealed that $Ca_v1.2$ is required for early postnatal survival of auditory neurons. In summary, $Ca_v1.2$ and $Ca_v1.3$ are both essential for the integrity of the auditory brainstem but differ in their requirement for the proper physiological function of auditory neurons.

Experimental Procedures

Animals—*Cacna1c*$^{fl/fl}$ mice (23) and the Cre-driver line *Egr2*::*Cre* (37) were described previously. Homozygous *Cacna1c*$^{fl/fl}$ mice were crossed with mice containing the locus *Egr2*::*Cre* in the heterozygous state and the *Cacna1c*^{fl} locus in the homozygous state (*Cacna1c*$^{fl/fl}$). Consequently, 50% of the offspring had the genotype *Egr2*::*Cre*;*Cacna1c*$^{fl/fl}$ (abbreviated *Cacna1c*^{Egr2}), and 50% had the genotype *Cacna1c*$^{fl/fl}$. The latter served as littermate controls. Mice were maintained at a C57BL/6 background, and animals of both sexes were used. The day of birth was taken as postnatal day 0 (P0). All protocols were in accordance with the German Animal Protection Law and approved by the local animal care and use committee (Landesamt für Verbraucherschutz und Lebensmittelsicherheit (LAVES), Oldenburg Regierungspräsidium (RP), Tübingen Landesuntersuchungsamt (LUA), Koblenz). The protocols also followed the National Institutes of Health guidelines for the care and use of laboratory animals.

Immunohistochemistry and Nissl Staining—Fluorescent immunohistochemistry was performed as described previously (33, 38). The antibodies applied were: polyclonal rabbit anti-VGlut1 (1:1,500, gift from Dr. S. El Mestikawy, Creteil, France), monoclonal rabbit anti-p-CREB (1:500, ID code 9198, Cell Signaling Technology, Danvers, MA), polyclonal rabbit anti-NFATc4 (1:200, HPA-031641, Sigma-Aldrich), polyclonal rabbit anti-p75NTR (1:500, AB1554, Millipore, Darmstadt, Germany), polyclonal goat anti-Sort1 (1:500, AF2934, Novus Biologicals, Littleton, CO), rabbit polyclonal anti-Iba1[7] (1:1,000, ID code 234003, Synaptic Systems, Göttingen, Germany), mouse monoclonal anti-NeuN (1:1,000, ab104224, Abcam, Cambridge, United Kingdom), and rabbit polyclonal anti-Kcnma1 (1:200, HPA-05464, Sigma-Aldrich). Nuclear staining was carried out with TO-PRO®-3 according to the manufacturer's instructions (T3605, Molecular Probes, Waltham, MA). The specificity of the antibodies used was given by analyses and reliable information from the manufacturer: Sigma prestige antibodies anti-NFATc4 and anti-Kcnma1 were tested thoroughly by immunohistochemistry against hundreds of normal and disease tissues in the human protein atlas; anti-p-CREB was tested by Western blot analysis; the specificity of anti-p75NTR is routinely evaluated by immunoprecipitation; anti-Sort1 was tested by direct ELISA and Western blotting; and anti-Iba1 and anti-NeuN were tested by immunohistochemistry and Western blotting. Anti-p75NTR and anti-NeuN are also listed in a collection of trustworthy antibodies by the Journal of Comparative Neurology. In addition, the subcellular localization of detected proteins was taken into account and met expectations (p-CREB in the nucleus; NeuN in the nucleus of neurons, *i.e.* no colocalization with microglia marker Iba1; Sort1 in the Golgi complex). Antibodies were diluted as indicated in carrier solution containing 1% bovine serum albumin, 1% goat serum, and 0.3% Triton X-100 in PBS, pH 7.4. For staining with goat anti-Sort1, a carrier without goat serum was used. Free-floating 30-μm-thick cryosections were incubated overnight at 7 °C, washed three times in PBS, and incubated in carrier solution with Alexa Fluor dye-coupled secondary antibodies (diluted 1:1,000, Invitrogen) for 1 h at room temperature. Finally, slices were washed and mounted onto gelatin-coated slides. Immunohistochemistry of neonatal tissue (P0–P4) was performed on-slide. To obtain optimal staining results for p-CREB, NFATc4, Sort1, Iba1, and Kcnma1 staining, antigen retrieval was performed using standard 10 mM trisodium citrate buffer, pH 6, treatment for 2 min. Images were taken with a BZ-8100E fluorescence microscope (Keyence, Neu-Isenburg, Germany) or with a TCS SP2 confocal laser scanning microscope (Leica, Wetzlar, Germany). Files were obtained using the Keyence BZ observation software or the Leica confocal software and processed in Adobe Photoshop CS6 (Adobe Systems, San Jose, CA).

Quantification of Kcnma1 immunosignals was performed with ImageJ (National Institutes of Health). A region of interest of 70 × 70 μm was defined within the central lateral superior olive (LSO) as well as outside the superior olivary complex (SOC) for background subtraction. Gray values were calculated and statistical analysis was performed using two-tailed Student's t test after testing for Gaussian distribution of the data sets with SPSS, version 21.0 (IBM Corp.). In the case of a non-Gaussian distribution, a Mann-Whitney U test was performed.

Nissl staining was performed on consecutive 30-μm-thick sections. The volume of auditory nuclei was calculated by multiplying the outlined area with the thickness of each section. Three young adult animals (P25–P30) and two young animals (P0 and P4) were used from each genotype. Analysis was carried out blind to the respective genotype. Sections were then analyzed using ImageJ, and statistical analysis was performed as mentioned above.

Quantitative RT-PCR Analysis—SOC tissue was collected from P2 animals as described (39). Briefly, 200-μm-thick brainstem slices were used to dissect the SOC from both sides under visual inspection. Tissue was stored at −80 °C until further use. For RNA isolation, SOC tissue from five animals was pooled to obtain sufficient yield per biological replicate. Two biological replicas were prepared for each genotype. Total RNA was extracted using the innuPREP RNA mini kit (Analytik Jena, Jena, Germany). cDNA was synthesized following the protocol of the RevertAid RT kit (Fermentas, Waltham, MA). To confirm Cre-mediated deletion of exons 14 and 15 in the dissected SOC tissue of *Cacna1c*^{Egr2} mice, RT-PCR was performed as described previously (23) with the primer pair VS11 (CTGGAATTCCTTGAGCAACCTTGT) and VS16 (AATTTCCACAGATGAAGAGGATG). GAPDH was amplified using the primers GAPDH forward (AATTTCCACAGATGAAGA GGATG) and GAPDH reverse (CTTGGCAGCACCAGTGGATG).

Quantitative RT-PCR was performed on a LightCycler 96 system (Roche) using the FastStart Essential DNA Green Master (Roche) containing SYBR Green. Primers used were as follows: RPL3 forward (GGTTTGCGCAAAGTTGCCTG), RPL3 reverse (ACCATCTGCACAAAGTGGTC), Fas forward (CCAGAAATCGCCTATGGTTG), Fas reverse (GTCATGTCTTCAGCAATTCTC), FasL forward (GACAGCAGTGCCACTTCATC), FasL reverse (ACTCCAGAGATCAGAGCGGT), p75NTR forward (AGACCTCATAGCCAGCACAG), p75NTR reverse (ACTGTAGAGGTTGCCATCAC), Sort1 forward (TTGATGACCTCAGTGGCTCAG), and Sort1 reverse (CCAAACATACTGCTTTGTGG). Each reaction was run in triplicate with the following thermocycling protocol: 95 °C for 5 min, 95 °C for 10 s, 60 °C for 10 s, and 72 °C for 10 s for a total of 45 cycles. Additionally, melting curves were generated to verify specificity of products. Samples were analyzed using the method of Pfaffl (40). All values were normalized to *RPL3* and reported as fold change in expression of *Cacna1c*^{Egr2} compared with *Cacna1c*$^{fl/fl}$. Statistical analysis was performed as mentioned above.

Extracellular Matrix Immunohistochemistry and Determination of Cell Diameters—Control and *Cacna1c*^{Egr2} animals (P70, $n = 3, 3$) were perfused transcardially under deep CO_2 anesthesia with 100 ml of 0.9% NaCl and 0.1% heparin followed by 100 ml of fixative containing 4% paraformaldehyde and 0.1% glutaraldehyde in 0.1 M PBS, pH 7.4. Brains were removed from the skull and postfixed in the same fixation solution overnight. The tissue was cryoprotected in 30% sucrose containing 0.01% sodium azide. 30-μm-thick coronal sections were collected individually in PBS containing 0.1% azide. Before staining, the sections were pretreated with 60% methanol containing 1% H_2O_2 for 30 min following a blocking step with a blocking solution containing 2% BSA, 0.3% milk powder, and 0.5% donkey serum in PBS-Tween (0.05%) for 1 h. All antibodies, incubated in the same blocking solution overnight at 4 °C, were applied as follows: a polyclonal rabbit anti-aggrecan antibody (1:1,000, AB1031, Millipore) that recognizes an epitope within amino acids 1177–1326 near the central domain of aggrecan at chondroitin sulfate glycosaminoglycan binding sites (41); a monoclonal mouse anti-brevican antibody (1:1000, BDB610894 clone2, BD Biosciences), detecting a 50-kDa N-terminal fragment and full-length brevican (41); and a polyclonal sheep anti-neurocan antibody (1:1,000, AF5800, R&D Systems) recognizing full-length neurocan (42).

Visualization of primary antibodies was performed by Cy3-conjugated anti-rabbit, anti-goat, anti-sheep, or anti-mouse antibodies raised in donkeys (1:1,000, Dianova). Image stacks were taken with a BZ-9000 fluorescence microscope (Keyence). Cell diameters were determined on full focus image stacks. Based on the neurocan immunoreaction in about 10 consecutive sections, cell diameters were measured of 10 principal cells/section using the BZ analyzer software. Statistical analysis was performed with SigmaPlot 12.5 software (Systat Software GmbH) by performing a Mann-Whitney *U* test.

Auditory Evoked Brainstem Responses and Otoacoustic Emissions—Auditory brainstem responses (ABR) and distortion product otoacoustic emission (DPOAE) were recorded in adult mice anesthetized with a mixture of ketamine hydrochloride (75 mg/kg body weight, Pharmacia, Erlangen, Germany) and xylazine hydrochloride (5 mg/kg body weight, Bayer, Leverkusen, Germany). Electrical brainstem responses to free field click (100 μs), noise burst (1 ms), and pure tone (3 ms with 1-ms ramp) stimuli were recorded with subdermal silver wire electrodes at the ear, the vertex, and the back of the animals. After amplification and bandpass filtering (200 Hz–5 kHz), signals were averaged for 64–256 repetitions at each sound pressure level presented (usually 0–100 db SPL in steps of 5 db). Thresholds were determined by the lowest sound pressure that evoked visually distinct potentials from above threshold to near threshold. The cubic $2f1 - f2$ DPOAE was measured for $f2 = 1.24 \times f1$ and L2 = L1–10 db. Emission signals were recorded during sound presentation of 260 ms and averaged four times for each sound pressure and frequency presented. First, the $2f1$-$f2$ distortion product amplitude was measured with L1 = 50 db SPL and $f2$ between 4 and 32 kHz. Subsequently, the $2f1$-$f2$ distortion product amplitude was measured for L1 ranging from −10 to 65 db SPL at frequencies of $f2$ between 4.0 and 32.0 kHz.

Average ABR wave curves are presented as mean ± S.E. Peak amplitudes and latencies were collected, grouped in clusters of similar peak amplitudes and latencies, and averaged for ABR wave input-output analysis. Clusters of peaks were found at average latencies $n0.9$-$p1.2$ (wave I), $n1.5$-$p2.2$ (wave II), $n2.9$-$p3.5$ (wave III), and $n3.9$-$p4.9$ (wave IV) (n is negative peak, p is positive peak, and the number is the peak latency in ms). The differences of the mean were compared for statistical significance by Student's t test, α-levels corrected for multiple testing by Bonferroni-Holms, and two-way analysis of variance (GraphPad Prism 2.01). Statistical significance was tested at $\alpha = 0.05$, and the resulting p values are reported in the text and in Fig. 8.

Electrophysiology—Patch clamp recordings in the whole-cell configuration were performed in acutely prepared slices on principal LSO neurons showing an I_H current (43). Animals were decapitated at P12 ± 2, and their brains were removed quickly. Coronal brainstem slices containing the superior olivary complex (270-μm thick, 1–2 slices/animal) were cut on a vibratome (VT-1200 S, Leica) in an ice-cold preparation solution (composition in mM: $NaHCO_3$, 26; NaH_2PO_4, 1.25; KCl,

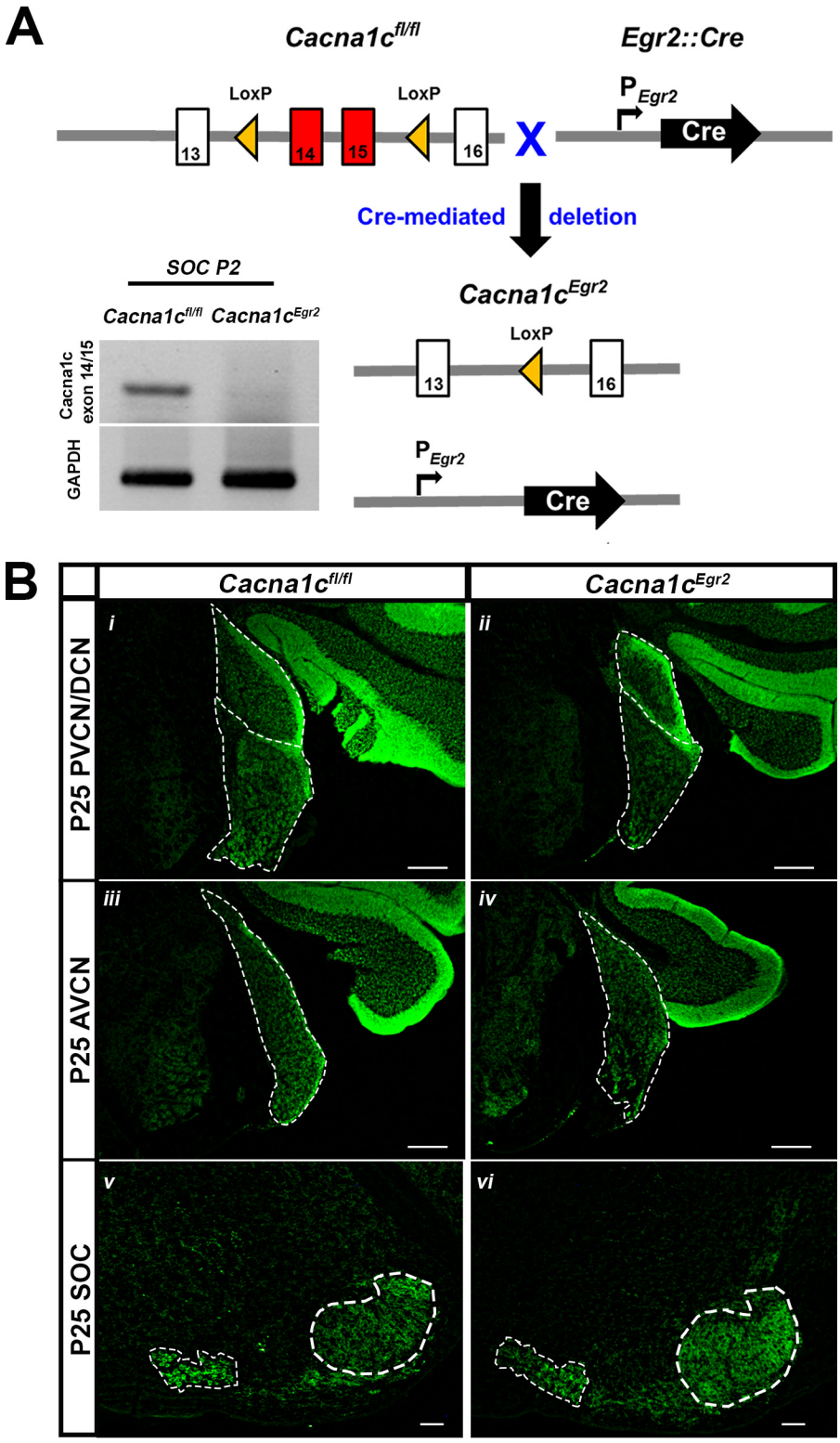

FIGURE 1. **Normal gross morphology of CNC and SOC in *Cacna1c*^{Egr2} mice.** *A*, schematic drawing of the mouse lines used. *Inset*, RT-PCR experiments demonstrating the absence of *Cacna1c* exons 14 and 15 containing mRNAs in the SOC. *B*, VGlut1 immunoreactivity in coronal brainstem sections of P25 *Cacna1c*$^{fl/fl}$ (*i*, *iii*, and *v*) and *Cacna1c*^{Egr2} mice (*ii*, *iv*, and *vi*) indicating normal gross morphology of CNC and SOC nuclei. Dorsal is *up*, and lateral is to the *right*. *Scale bars*, 100 μm.

2.5; $MgCl_2$, 1; $CaCl_2$, 2; D-glucose, 260; sodium pyruvate, 2; *myo*-inositol, 3; and kynurenic acid, 1; pH 7.4 when bubbled with 95% O_2 and 5% CO_2) and then stored at 37 °C for 1 h in artificial CSF (composition in mM: NaCl, 125; $NaHCO_3$, 25; NaH_2PO_4, 1.25; KCl, 2.5, $MgCl_2$, 1; $CaCl_2$, 2; D-glucose, 10; sodium pyruvate, 2; myoinositol, 3; and ascorbic acid 0.44; pH 7.4 when bubbled with 95% O_2 and 5% CO_2). Thereafter, slices were stored at room temperature before being transferred into

TABLE 1

Quantification of structural changes in the three CNC nuclei and in two SOC nuclei of young adult *Cacna1c*$^{fl/fl}$ and *Cacna1c*^{Egr2} mice

Values are means ± S.D.

	Volume				Cell number			
	Cacna1c$^{fl/fl}$	*Cacna1c*^{Egr2}	*p* value	% reduction	*Cacna1c*$^{fl/fl}$	*Cacna1c*^{Egr2}	*p* value	% reduction
DCN	0.2109 ± 0.0168	0.1545 ± 0.0140	0.000422	26.7				
PVCN	0.0884 ± 0.0211	0.0900 ± 0.0038	0.859					
AVCN	0.1416 ± 0.0136	0.1247 ± 0.0086	0.028	11.9				
MNTB	0.0373 ± 0.0062	0.0294 ± 0.0032	0.019	21.2	2906.17 ± 132.36	2227.83 ± 318.81	0.001	23.3
LSO	0.0253 ± 0.0029	0.0164 ± 0.0045	0.002	35.2	1511.8 ± 158.7	704.3 ± 17.2	0.0000001	53.4

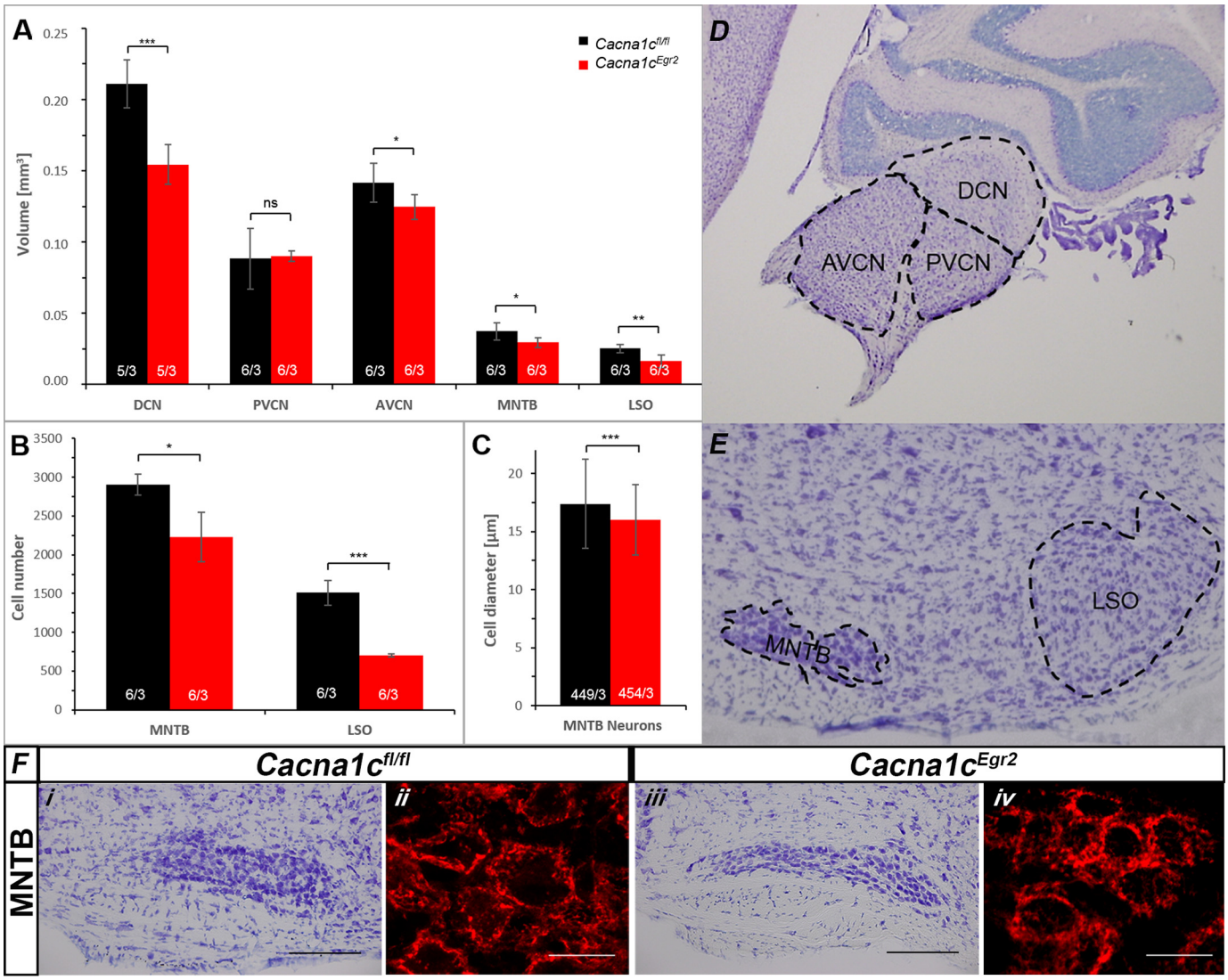

FIGURE 2. **Structural alterations in young adult auditory brainstem nuclei.** *A*, in *Cacna1c*^{Egr2} mice, the volume of DCN, AVCN, LSO, and MNTB was significantly decreased, whereas no changes were observed in the PVCN arising from rhombomere 4. *B*, LSO and MNTB of *Cacna1c*^{Egr2} mice displayed a lower numbers of cells. *C*, cell diameter was reduced in MNTB neurons of *Cacna1c*^{Egr2} mice. Determination of cell diameter in P70 MNTB neurons was performed using neurocan-labeled cells (see Fig. 3). 449 (*Cacna1c*$^{fl/fl}$) and 454 (*Cacna1c*^{Egr2}) cells from three animals were analyzed. *D*, volume of CNC nuclei was analyzed in P25 Nissl-stained parasagittal section series (5 or 6 nuclei from 3 animals). *E*, volume and cell number of SOC nuclei were analyzed in P25 Nissl-stained coronal sections (six nuclei from three animals). As a test for statistical significance, Student's *t* test (volume and cell number) or Mann-Whitney *U* test (diameter) was used. Color coding: *black* = control *Cacna1c*$^{fl/fl}$ mice; *red* = *Cacna1c*^{Egr2}mice. *, $p \leq 0.01$; **, $p \leq 0.05$; ***, $p \leq 0.001$; *ns*, not significant. *F*, representative examples of the morphological changes in *Cacna1c*^{Egr2} mice. In Nissl-stained sections the MNTB appears more stretched and narrowed compared with slices of control mice (*i* and *iii*, *scale bars* = 200 μm). Single MNTB cells of *Cacna1c*^{Egr2} mice are also clearly smaller in aggrecan-stained specimens (*ii* and *iv*, *scale bars* = 20 μm). Dorsal is *up*, and lateral is to the *right* with the exception of *D*, where dorsal is *up*, and caudal to the *right*.

a recording chamber in which they were continually superfused with artificial CSF. The chamber was mounted on an upright microscope (Eclipse E600FN, Nikon, Tokyo, Japan) equipped with differential interference contrast optics (Nikon objectives: 4× CFI Achromat, 0.1 NA; 60× CFI Fluor W, 1.0 NA) and an infrared video camera system (CCD camera C5405-01 (Hamamatsu, Herrsching, Germany) and PC frame-grabber card, pciGrabber-4plus (PHYTEK, Mainz, Germany)). Patch pipettes were pulled from borosilicate glass capillaries (GB150(F)-8P, Science Products, Hofheim, Germany) with a

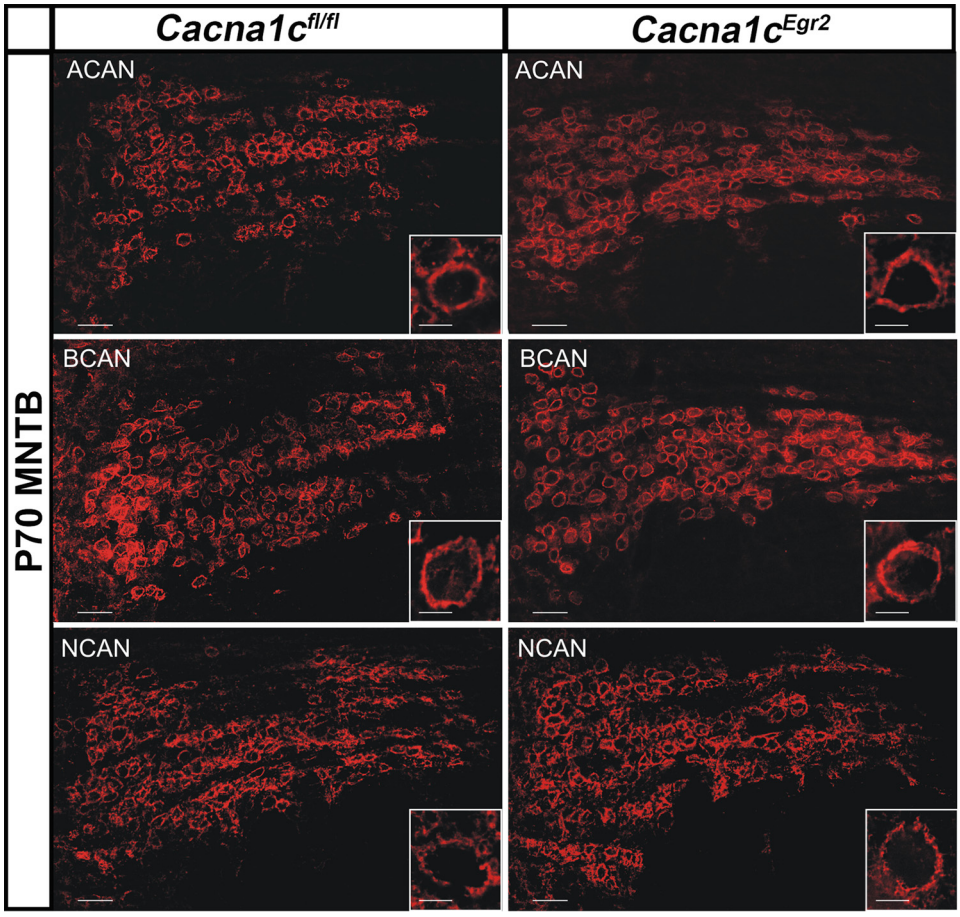

FIGURE 3. **Normal PN formation in *Cacna1c*^{Egr2} mice.** Immunoreactivity of the MNTB for the proteoglycans aggrecan (*ACAN*), brevican (*BCAN*), and neurocan (*NCAN*). *Insets* depict single representative MNTB neurons. No differences were observed in PN composition or structure between *Cacna1c*^{Egr2} mice and littermate controls. Dorsal is *up*, and lateral is to the *left*. *Scale bars*, 50 μm; in *insets*, 10 μm.

TABLE 2

Biophysical properties of *Cacna1c*$^{fl/fl}$ and *Cacna1c*^{Egr2} mice

Values are means ± S.E. Action potential (AP) properties (rows 4–8) are measured at the first appearing action potential. V_{rest}, resting membrane potential; pF, picofarad.

	Cacna1c$^{fl/fl}$	*Cacna1c*^{Egr2}	*p* value
Number of cells	20	22	
Input resistance (megohms)	44.3 ± 2.8	47.0 ± 3.3	0.27
V_{rest} (mV)	−71.2 ± 1.3	−71.9 ± 1.0	0.66
Firing onset (ms)	33.2 ± 0.4	32.8 ± 0.2	0.83
Firing threshold (mV)	−46.1 ± 1.6	−44.4 ± 1.4	0.43
Peak amplitude (mV)	20.8 ± 3.8	26.3 ± 2.6	0.22
Half-width (ms)	0.6 ± 0.06	0.5 ± 0.03	0.03
Afterhyperpolarization (mV)	−63.6 ± 2	−59.9 ± 1.6	0.15
Capacitance (pF)	25.7 ± 1.3	26.3 ± 1.2	0.71
Membrane time constant (ms)	0.5 ± 0.08	0.7 ± 0.07	0.2
0–63% rise time (ms)	2.6 ± 0.2	2.6 ± 0.2	0.7
Single firing (%)	76.4	81.3	
Multiple firing (%)	23.6	18.7	
Number of AP elicited by 500 pA current injection	14.7 ± 3.3	10.6 ± 6.2	0.5

horizontal puller (P-87, Sutter Instruments, Novato). They had resistances of 3–6 meghoms when filled with artificial intracellular solution (composition in mM: potassium gluconate, 140; EGTA, 5; $MgCl_2$, 1; HEPES, 10; Na2ATP, 2; and Na2GTP, 0.3; pH 7.2 with KOH; liquid junction potential, 15.4 mV) and connected to an EPC 10 patch clamp amplifier (HEKA Elektronik, Lambrecht, Germany). The liquid junction potential was corrected online. Sample frequency was 20 kHz, and cut-off frequency of low-pass filtering was 10 kHz. Series resistance was routinely compensated by 10–30%.

The biophysical properties of the neurons were assessed at room temperature. To analyze the passive membrane properties and spiking characteristics, recordings were performed in current clamp mode, and 200-ms-long rectangular current pulses were injected from −200 to +450 pA in 50-pA steps.

Synaptic responses were analyzed from voltage clamp recordings at a holding potential of −70 mV and nearly physiological temperature (36 ± 1 °C). To measure evoked inhibitory postsynaptic currents (eIPSCs), a theta glass electrode (TST150-6, World Precision Instruments) with a tip diameter of 10–20 μm was filled with artificial CSF and placed lateral to the medial nucleus of the trapezoid body (MNTB). Biphasic pulses (100 μs each) were applied through a programmable pulse generator (STG4004, Multi Channel Systems GmbH, Reutlingen, Germany). The amplitude of the stimulus pulses was 500–3,000 μA and was set to achieve stable synaptic responses with an amplitude jitter of <50 pA. To determine the synaptic performance of the MNTB-LSO connection and the size of the readily releasable pool, five 100-pulse trains at 100 Hz were applied with a 59-s pause between trains. The peak amplitude of the first eIPSC in a trial was set to 100% for normalization.

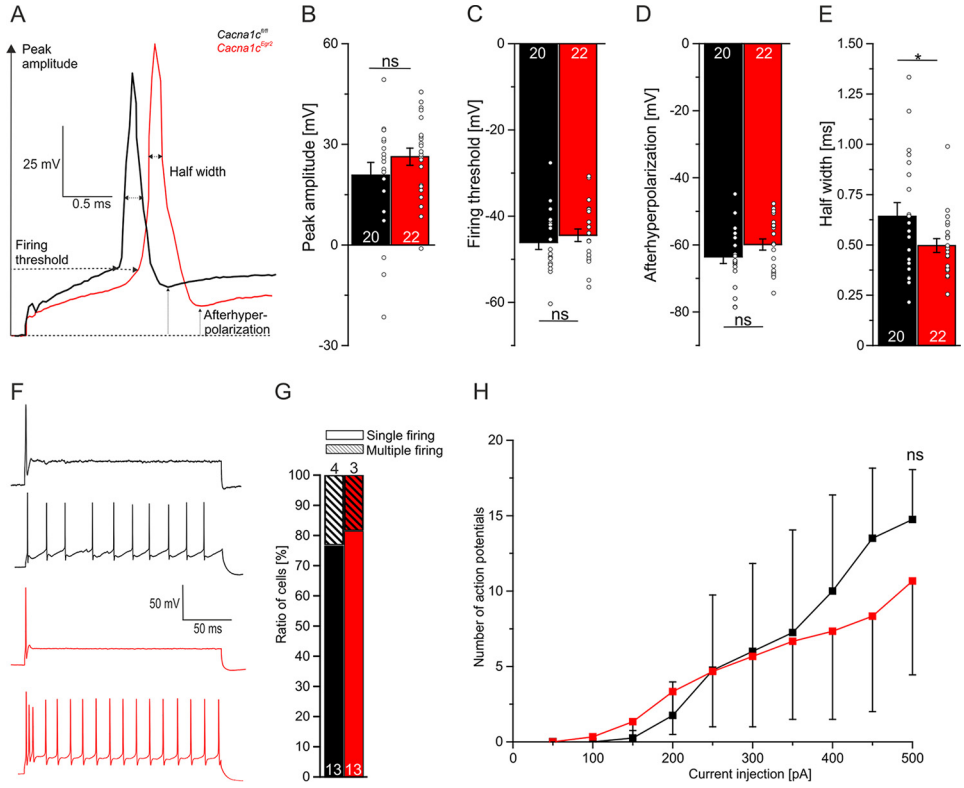

FIGURE 4. **Narrowed half-width of spikes in LSO neurons of *Cacna1c*^{Egr2} mice.** *A*, exemplary traces of first evoked spikes of a *Cacna1c*$^{fl/fl}$ (*black*) and a *Cacna1c*^{Egr2} (*red*) in response to a +100 pA rectangular current injection illustrating the analyzed parameters. Peak amplitude (*B*), firing threshold (*C*), and afterhyperpolarization (*D*) did not differ significantly between genotypes. *E*, in contrast, there was a significant difference in the half-width, which was narrowed by 17% in *Cacna1c*^{Egr2} mice. *, $p < 0.05$; **, $p < 0.01$; ***, $p < 0.001$; two-sided Student's *t* test. *ns*, not significant. *F*, exemplary traces of evoked single and multiple firing LSO neurons in both *Cacna1c*$^{fl/fl}$ (*black*) and *Cacna1c*^{Egr2} (*red*) upon rectangular current injection of +500 pA for 200 ms. *G*, the great majority of LSO neurons fired a single spike during a 200-ms-long depolarizing pulse, independent of the genotype. *Solid bar*, single firing neurons; *dashed bar*, multiple firing neurons. *H*, the number of action potentials elicited upon increasing the current injections did not differ significantly between genotypes.

Miniature Events—To determine synaptic release properties, inhibitory and excitatory miniature events (mIPSCs and mEPSCs) were recorded simultaneously with 50-kHz sampling. Miniature recordings were performed in the presence of a 1 μM tetrodotoxin (Sigma-Aldrich), which was bath-applied for 5 min before 6-min recordings were obtained. Because of the ion concentrations in the artificial CSF and the artificial intracellular solution, the equilibrium potentials, E_{Cl}^- and E_{Na}^+, amounted to approximately −110 and +93 mV, respectively, thus being considerably more negative and positive than the holding potential of −70 mV.

Data Analysis—The biophysical membrane properties were analyzed using pCLAMP10 (Molecular Devices, Sunnyvale, CA) and Fitmaster (HEKA Elektronik). eIPSC and eEPSC peak amplitudes were analyzed with a customized plug-in for Igor-Pro 6.32 (WaveMetrics, Portland, OR). mEPSC and mIPSC data analysis was performed with MiniAnalysis 6.0.3 (Synaptosoft, Decatur, GA).

Statistics—To assess statistical significance, the WinSTAT package was used (R. Fitch Software, Bad Krotzingen, Germany). Data were checked for Gaussian distribution (Kolmogorov-Smirnov) and outliers (more than 4× S.D. above or below the mean) were excluded. A two-tailed Student's *t* test was performed. Error bars in the diagrams illustrate S.E. Dot plots of single values are added to the bar charts in the diagrams to illustrate the distribution.

Results

Structural Abnormalities in the Adult SOC of Cacna1c^{Egr2} *Mice*—Functional expression of $Ca_v1.2$ has been demonstrated previously in the auditory brainstem (36). To study the role of this channel type in the cochlear nucleus complex (CNC) and SOC, we used a recently generated *Egr2*::*Cre*;*Cacna1c*$^{fl/fl}$ (*Cacna1c*^{Egr2}) mouse model (44) in which Cre-mediated recombination results in deletion of exons 14 and 15 of *Cacna1c* in rhombomeres 3 and 5 (Fig. 1*A*). Accordingly, mRNA containing exons 14 and 15 is undetectable in the SOC tissue (Fig. 1*A*, *inset*). This is in agreement with the lack of protein in the auditory brainstem in this mouse line (44). Taken together, these data demonstrate that the *Egr2*::*Cre* driver line very efficiently recombines the *Cacna1c*$^{fl/fl}$ allele, which results in undetectable levels of $Ca_v1.2$ in auditory hindbrain neurons. In all experiments, *Cacna1c*$^{fl/fl}$ mice served as controls.

To investigate the functional consequences of $Ca_v1.2$ ablation, we probed the integrity of the young adult (P25–P30) CNC and SOC by fluorescent immunohistochemistry for VGlut1, which is strongly expressed in auditory brainstem nuclei (38, 45, 46) (Fig. 1*B*). No obvious alterations were detected in the CNC, and all three subdivisions, the anterior ventral cochlear nucleus (AVCN), the posteroventral cochlear nucleus (PVCN), and the dorsal cochlear nucleus (DCN) were clearly delineated (Fig. 1*B*, *i–iv*). However, quantitative analysis of Nissl-stained sections demonstrated a significant volume reduction of the

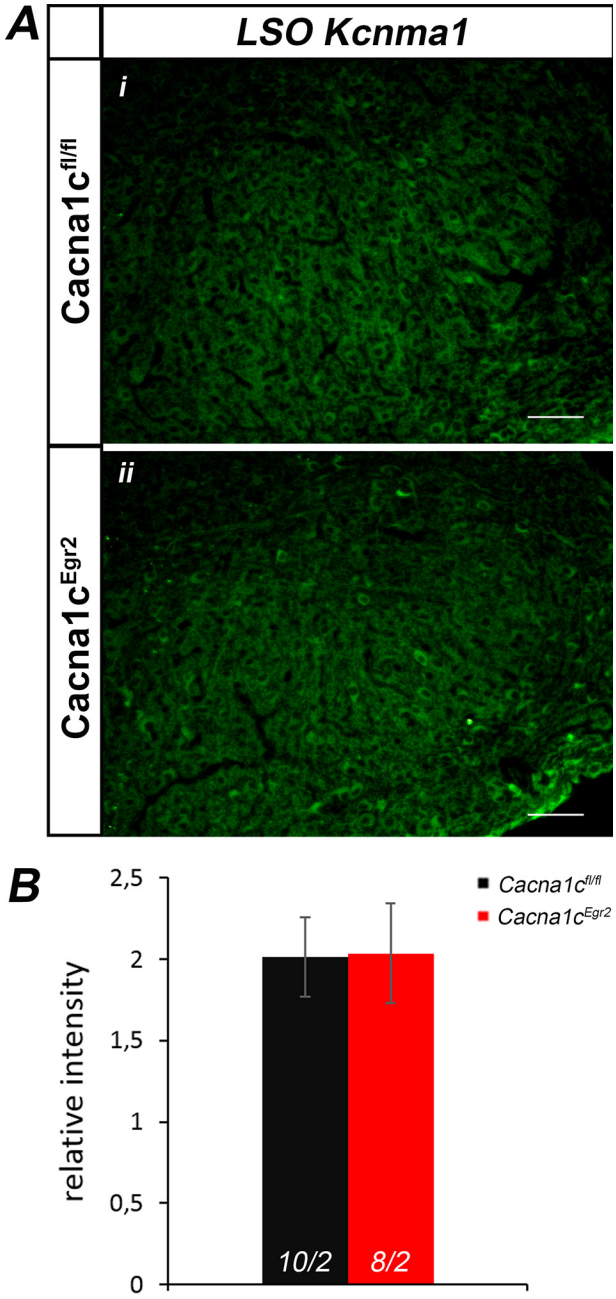

FIGURE 5. **No changes in Kcnma1 immunoreactivity in the LSO of *Cacna1c*^{Egr2} mice.** *A*, immunohistochemistry for Kcnma1 in the LSO of *Cacna1c*^{Egr2} (*i*) and control mice (*ii*) at P12. Dorsal is *up*, and lateral is to the *left*. *Scale bars*: 50 μm. *B*, quantification of the Kcnma1 signal in the LSO relative to fluorescence outside the SOC area (mean ± S.D., 8–10 LSO slices from two animals for each genotype). No difference in relative intensities was observed between the two genotypes. As a test for statistical significance, Student's *t* test was used. *Black*, control *Cacna1c*$^{fl/fl}$ mice; *red*, *Cacna1c*^{Egr2} mice. Dorsal is *up*, and lateral is to the *right*.

AVCN by 11.9% (control, 0.142 ± 0.014 mm^3; *Cacna1c*^{Egr2}, 0.125 ± 0.009 mm^3; $p = 0.028$) and the DCN by 26.7% (control, 0.211 ± 0.017 mm^3; *Cacna1c*^{Egr22}, 0.154 ± 0.014 mm^3; $p = 0.00042$) (Table 1). No volume change was observed for the PVCN (Fig. 2*A* and Table 1), which is in agreement with its origin mainly from rhombomere 4 (47). Major SOC nuclei, such as the LSO or the MNTB, appeared smaller in *Cacna1c*^{Egr2} mice compared with control littermates when labeled for VGlut1 or Nissl stained (Fig. 1*B*, *v* and *vi*, and Fig. 2*F*, *i* and *iii*). Quantitative analysis revealed a volume reduction of the LSO by 35.2% (control, 0.025 ± 0.003 mm^3; *Cacna1c*^{Egr2}, 0.016 ± 0.004 mm^3; $p = 0.002$) and the MNTB by 21.2% (control, 0.037 ± 0.006 mm^3; *Cacna1c*^{Egr22}, 0.029 ± 0.003 mm^3; $p = 0.019$) (Fig. 2*A* and Table 1). There was no difference between control animals and heterozygous knock-out animals with only one *Cacna1c*^{fl} allele (data not shown).

Because the strongest volume decrease was observed in the SOC, we focused our subsequent analyses on this structure. Cell counts revealed that the decreased volume in the LSO and MNTB was due to a reduced number of neurons (LSO: control, 1,511.8 ± 158.7; *Cacna1c*^{Egr2}, 704.3 ± 17.2 (−53.4%), $p = 10^{-7}$; MNTB: control, 2,906.17 ± 132.36; *Cacna1c*^{Egr2}, 2,227.83 ± 318.81 (−23.3%), $p = 0.001$) (Fig. 2*B* and Table 1). Furthermore, analysis of the soma size of MNTB neurons revealed a slight but significant 8% reduction in cell diameter (control, 17.4 ± 3.8 μm; *Cacna1c*^{Egr2}, 16.0 ± 3.01 μm; $p = 0.001$, Mann-Whitney *U* test) (Fig. 2*C*). This reduction was also visible in aggrecan-immunopositive MNTB neurons (Fig. 2*F*, *ii* and *iv*). Taken together, these anatomical data indicate a crucial role of $Ca_v1.2$ in the proper formation of the mature CNC and SOC. Significantly, the structural phenotype resembles the changes reported after the loss of $Ca_v1.3$, and again, the SOC was affected more heavily than the CNC (33, 34).

Immunohistochemical Analysis of the Extracellular Matrix in Cacna1c^{Egr2} *Mice*—Previous studies have revealed the prominent appearance of perineuronal nets (PNs) around the soma of virtually every principal MNTB neuron (41), in agreement with the high expression of genes encoding the proteoglycans brevican, aggrecan, and versican, hyaluronan and proteoglycan link protein 1, and tenascin R in the developing SOC (48, 49). As the extracellular matrix of PNs is assumed to be involved in Ca^{2+} signaling, diffusion, and channel activity (50–52), and as VGCCs have been implicated in the formation of PNs (53), we analyzed the expression of the major proteoglycans, aggrecan, brevican, and neurocan, in the MNTB at P70. At this age, PNs are fully developed, and any alteration should therefore clearly be recognizable. All three PN components strongly decorated MNTB neurons in both control animals and *Cacna1c*^{Egr2} mice (Fig. 3). No difference was obvious between genotypes. These data suggest that the formation of PNs around MNTB neurons is independent of the presence of $Ca_v1.2$.

Half-width of Action Potentials Is the Only Altered Biophysical Property of LSO Neurons in Cacna1c^{Egr2} *Mice*—To assess whether loss of $Ca_v1.2$ affects the functional characteristics of LSO neurons, several biophysical properties were analyzed. For this purpose, we performed current clamp recordings in acute slices of P12 ± 2 control and *Cacna1c*^{Egr2} mice and determined passive and active membrane properties. The resting membrane potential (V_{rest}) did not differ between genotypes. Likewise, there was no difference in the input resistance, the membrane time constant, and the membrane capacitance (Table 2). Depolarizing current pulses of sufficient amplitude elicited action potentials in both genotypes in which the overshooting peak amplitudes did not differ (Fig. 4, *A* and *B*, and Table 2). Likewise, both genotypes displayed similar firing thresholds (Fig. 4, *A* and *C*, and Table 2), and similar afterhyperpolarization amplitudes (Fig. 4*D* and Table 2). The 0–63% rise time of

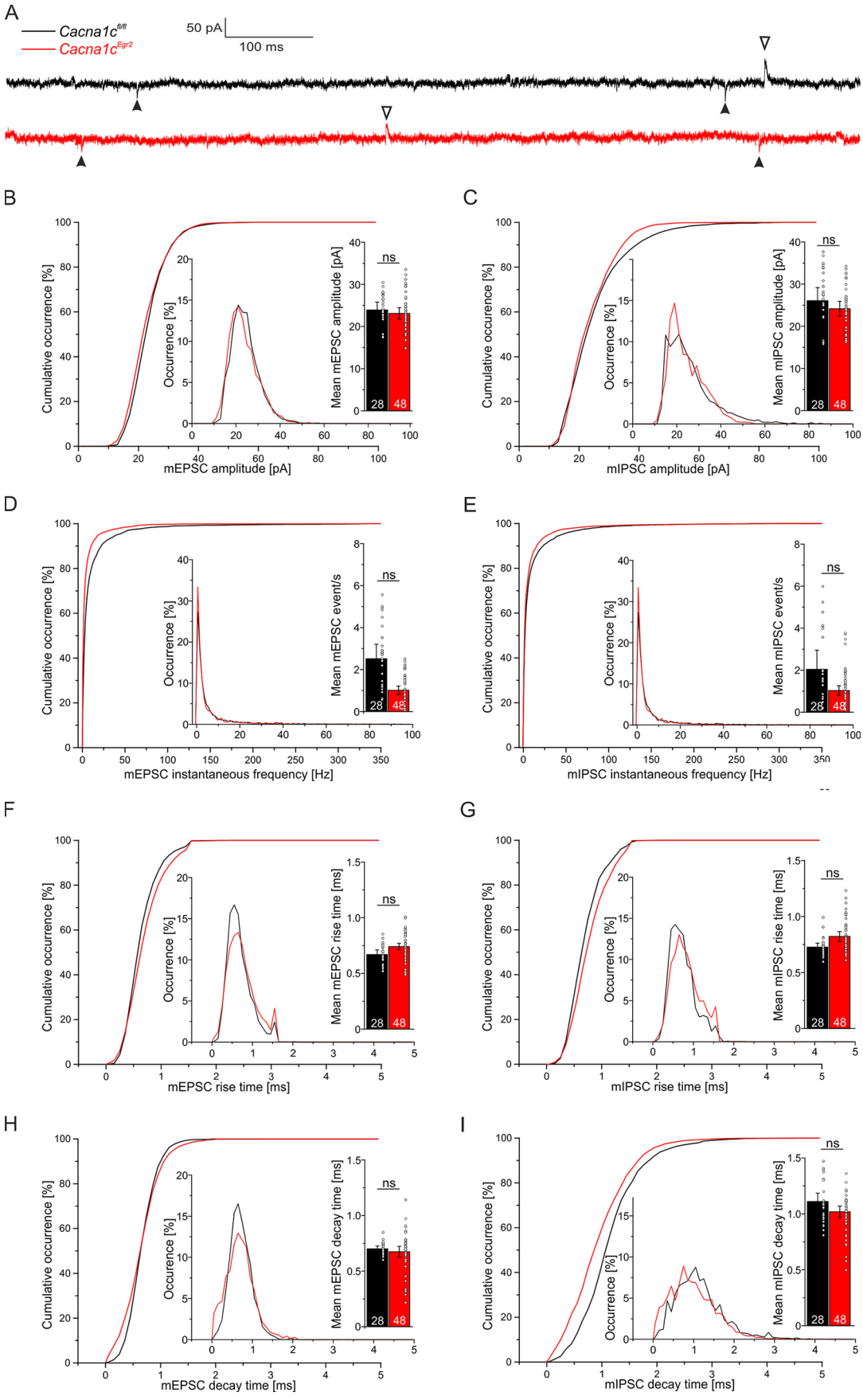

TABLE 3
Properties of excitatory and inhibitory miniature events in *Cacna1c*$^{fl/fl}$ and *Cacna1c*^{Egr2} mice
Values are means ± S.E.

	Cacna1c$^{fl/fl}$	*Cacna1c*^{Egr2}	*p* value
Number of cells	28	48	
mEPSC amplitudes (pA)	24.0 ± 1.8	23.1 ± 1.3	0.72
mIPSC amplitudes (pA)	26.1 ± 3.1	24.1 ± 1.8	0.56
mEPSC events/s	2.5 ± 0.7	1.0 ± 0.2	0.09
mIPSC events/s	2.0 ± 0.9	1.0 ± 0.2	0.33
mEPSC rise time (ms)	0.7 ± 0.04	0.7 ± 0.02	0.17
mIPSC rise time (ms)	0.7 ± 0.03	0.8 ± 0.04	0.16
mEPSC decay time (ms)	0.7 ± 0.02	0.7 ± 0.04	0.71
mIPSC decay time (ms)	1.1 ± 0.07	1.1 ± 0.05	0.31

responses to subthreshold depolarizations also did not differ (Table 2). However, a significant difference between genotypes was observed in the half-width of the action potentials, which was 17% narrower in the knockouts (Fig. 4, *A* and *E*, and Table 2). To check whether this change was associated with an altered expression of Ca^{2+}-activated potassium channels of the BK type, we probed expression of Kcnma1 in the LSO at P12. Kcnma1 represents the pore-forming α-subunit (54). Immunohistochemistry revealed low expression (Fig. 5*A*) with no quantitative difference between genotypes (Fig. 5*B*, control, 2.01 ± 0.25; *Cacna1d*^{Egr2}, 2.04 ± 0.31). The low abundance of Kcnma1 is in agreement with immunohistochemical results in the mouse auditory system (54) and argues against an important role for this protein in shaping the action potentials in this nucleus.

In mice lacking $Ca_v1.3$, the majority of LSO neurons display a multiple firing pattern during depolarizing pulses, in contrast to the controls (33). We also analyzed the firing pattern in *Cacna1c*^{Egr2} mice (Fig. 4*F*). Independent of the genotype, the majority of neurons fired a single action potential (Fig. 4*G* and Table 2), and consequently, multiple spiking was less abundant. Finally, the input-output curves of the few multiple firing neurons did not display significant differences (Fig. 4*H*). This implies that the firing pattern in response to current pulses of varying amplitude was unaltered upon $Ca_v1.2$ deletion. Together, these data reveal different requirements of $Ca_v1.3$ and $Ca_v1.2$ for the maturation of the biophysical parameter in principal LSO neurons.

Unaltered Neurotransmission to the LSO in Cacna1c^{Egr2} *Animals*—In a next series of experiments, we analyzed excitatory and inhibitory neurotransmission to LSO neurons. To do so, miniature postsynaptic currents were recorded over a period of 6 min during which several parameters were analyzed (Fig. 6 and Table 3). Neither in the excitatory nor the inhibitory inputs could we find a change in the amplitude of miniature currents (Fig. 6, *A–C*, and Table 3). Likewise, the frequency, rise time, and decay time of mEPSCs and mIPSCs were unaltered (Fig. 6, *D–I*, and Table 3). Together, these results are suggestive of unchanged transmitter vesicles in the presynaptic axon terminals and unchanged postsynaptic transmitter composition.

TABLE 4
Properties of short-term synaptic depression in *Cacna1c*$^{fl/fl}$ and *Cacna1c*^{Egr2} mice
Values are means ± S.E. RRP, readily releasable pool.

	Cacna1c$^{fl/fl}$	*Cacna1c*^{Egr2}	*p* values
Number of cells	12	15	
First eIPSC amplitude (pA)	515 ± 100	640 ± 110	0.42
Last eIPSC amplitude (pA)	175 ± 37	211 ± 42	0.54
RRP size (nA)	3.5 ± 0.6	5.8 ± 1.3	0.21
Release probability (%)	14.5 ± 0.8	13.3 ± 1.0	0.98

Finally, we analyzed the inhibitory neurotransmission between MNTB and LSO in acute slices upon electrical stimulation of the MNTB axons. Mean peak amplitudes of eIPSCs were 515 ± 100 pA in controls and 640 ± 110 pA in *Cacna1c*^{Egr2} mice, and these did not differ significantly from each other (Table 4). Upon high-frequency stimulation (100-Hz trains of 100 pulses), short-term depression was observed in both genotypes, and the time course was virtually the same (Fig. 7*A*). The amount of depression was ~60% for both control and knock-out mice, and the last peak amplitude in the train reached similar values (Fig. 7*B* and Table 4). From the high-frequency stimulation experiments, we also determined the size of the readily releasable pool and the release probability. We found no differences between genotypes (Fig. 7*C* and Table 4), which is indicative of an unaltered presynaptic release machinery in the MNTB axon terminals upon loss of $Ca_v1.2$.

Nearly Normal Auditory Brainstem Responses in Cacna1c^{Egr2} *Animals*—We next assessed the functional consequences of the loss of $Ca_v1.2$ for acoustic information processing. To do so, we analyzed ABRs and DPOAE. ABR thresholds for pure tone, click, and noise burst stimuli as well as DPOAE thresholds and amplitudes were similar for *Cacna1c*^{Egr2} and control animals (Fig. 8, *A–C*), demonstrating normal hearing sensitivity of the inner ear in *Cacna1c*^{Egr2} mice. Next, ABR waves (peak amplitudes and latencies) were analyzed, which are a characteristic sequence of negative (*n*) and positive (*p*) deflections (peaks), with each pair of *n* and *p* referred to as a wave (waves I–V). The summed activity of the auditory nerve gives rise to wave I, whereas wave II reflects the response of globular bushy cells in the CNC. Wave III originates mainly in the CNC and SOC. Finally, the lateral lemniscus and inferior colliculus appear to contribute to waves IV and V (55, 56). At 86 db SPL, ABR waves III and IV appeared to have smaller amplitudes in *Cacna1c*^{Egr2} animals than in controls when averaged across five animals (Fig. 8*D*). Fine analyses revealed that this difference was due to a significant increase in the interindividual variation of the latency of the negative peaks III and IV (Fig. 8*E*). When each animal was analyzed separately, no difference in amplitude was observed compared with control animals (Fig. 8*F*). These data indicate a higher interindividual variability in the conductance or wiring of the central auditory circuitry in the absence of $Ca_v1.2$ but otherwise normal ABRs. The results are in contrast

FIGURE 6. **Spontaneous synaptic release was not altered in LSO neurons of *Cacna1c*^{Egr2} mice.** *A*, exemplary traces of 1-s recordings at a holding potential of −70 mV of *Cacna1c*$^{fl/fl}$ (*black*) and a *Cacna1c*^{Egr2} (*red*). Spontaneous excitatory miniature events (mEPSC) are indicated by *solid arrowheads*, spontaneous inhibitory miniature events (mIPSC) are marked by *open arrowheads*. Cumulative occurrence of mEPSC amplitude (*B*), mIPSC amplitude (*C*), mEPSC instantaneous frequency (*D*), mIPSC instantaneous frequency (*E*), mEPSC rise time (*F*), mIPSC rise time (*G*), mEPSC decay time (*H*), and, mIPSC decay time (*I*) was not changed between genotypes. *Insets* show relative occurrence and mean values of each parameter. *ns*, not significant.

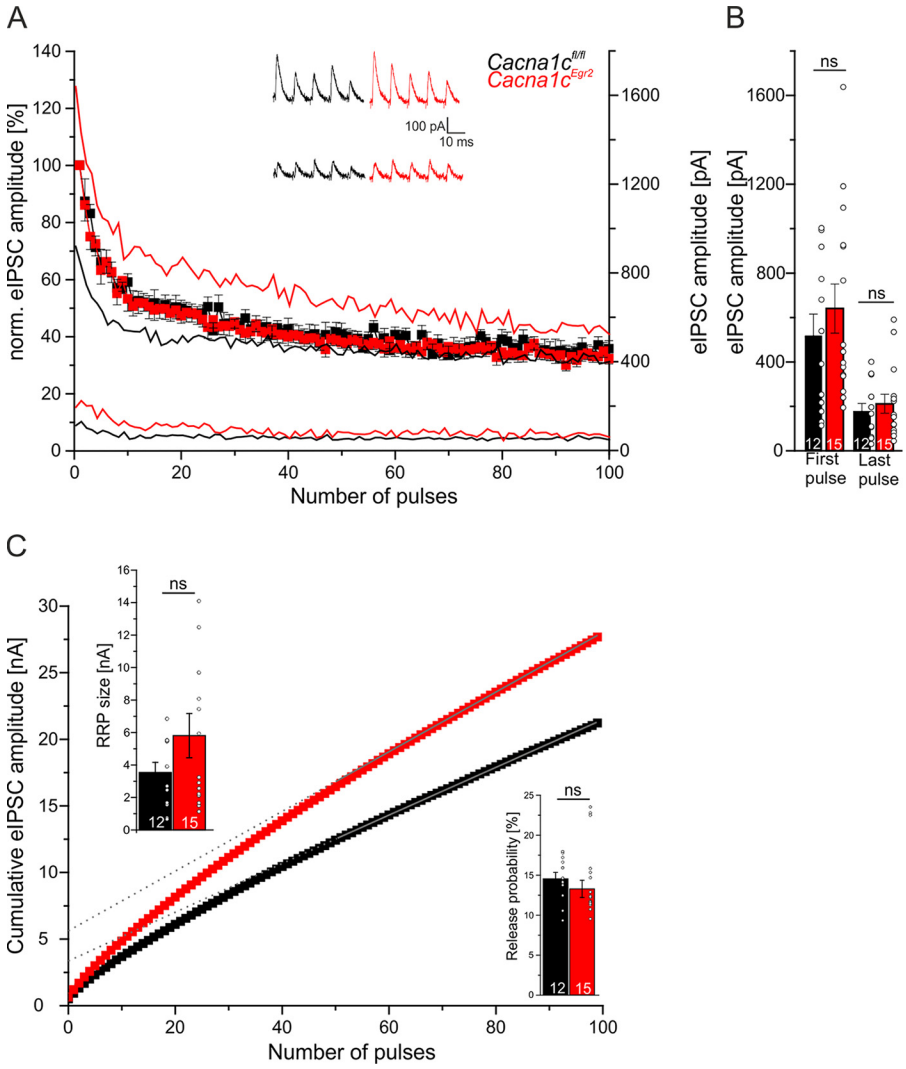

FIGURE 7. **Short-term synaptic depression did not differ between LSO neurons of *Cacna1c*$^{fl/fl}$ and *Cacna1c*^{Egr2} mice.** *A*, course of depression of normalized mean eIPSC amplitudes of *Cacna1c*$^{fl/fl}$ (*black*) and a *Cacna1c*^{Egr2} (*red*) LSO neurons was not altered upon 100-Hz stimulation for 1 s. *Solid lines* show individual cells, two for each genotype. Raw *traces* of the first and last five eIPSC amplitudes also show no obvious difference among the groups. *B*, the first and last eIPSC amplitude did not differ significantly between genotypes. *C*, cumulative eIPSC amplitude with back-extrapolated linear fits (*dotted gray line* (102)). *Insets* show that no differences in the size of the readily releasable pool (*RRP*) or the release probability were observed. *ns*, not significant.

to the findings in *Cacna1d*^{Egr2} mice, which showed a decreased amplitude for wave I between 50 and 75 db and increased amplitudes for waves II and III for stimulation amplitudes above 60 db (34). Thus, they point to distinct functions of $Ca_v1.2$ and $Ca_v1.3$ regarding the processing of acoustic information in the auditory brainstem.

Loss of $Ca_v1.2$ Causes Early Postnatal Death of SOC Neurons—Our anatomical analysis of the SOC in young adult *Cacna1c*^{Egr2} mice revealed a dramatic reduction in cell number. In mice, SOC neurons are born between embryonic days 9 and 14 (57) and have completed their migration by birth (58). Therefore, the observed reduction in neuron number may be due to defects in cell birth, migration, or postmigratory survival of neurons. To assess which of these steps requires $Ca_v1.2$, we analyzed the MNTB at P0, as this nucleus is the only clearly recognizable SOC structure in Nissl-stained sections at this age. Quantitative analysis revealed a trend to a decreased nuclear volume (control, 0.013 ± 0.0009 mm^3; *Cacna1c*^{Egr2}, 0.011 ± 0.0007 mm^3; $p = 0.241$) and a small, albeit significant decrease in the neuron number of *Cacna1c*^{Egr22} mice (control, 1,771 ± 94; *Cacna1c*^{Egr2}, 1,596 ± 23; $p = 0.041$) (Fig. 9 and Table 5).

As reported previously, ablation of $Ca_v1.3$ results in an abnormal LSO structure, which is observed already at P4 (33, 34). To investigate whether $Ca_v1.2$ is similarly required during early postnatal differentiation, we analyzed the MNTB at P4 as well. Quantitative analysis of Nissl-stained sections revealed significant differences in volume (control, 0.021 ± 0.001 mm^3; *Cacna1c*^{Egr2}, 0.013 ± 0.0002 mm^3; −39%, $p = 10^{-7}$) and neuron number (control, 2,041 ± 91; *Cacna1c*^{Egr2}, 1,217 ± 59; −40.4%, $p = 5 \times 10^{-6}$, Fig. 9 and Table 5). The drastic decline of ~40% in the neuron number between P0 and P4 reveals that MNTB neurons heavily depend on L-VGCC-mediated signaling for survival during the first postnatal days in mice. This time period occurs soon after circuit formation, which allows spontaneous activity arising in the cochlea to spread along the auditory pathway (59–61).

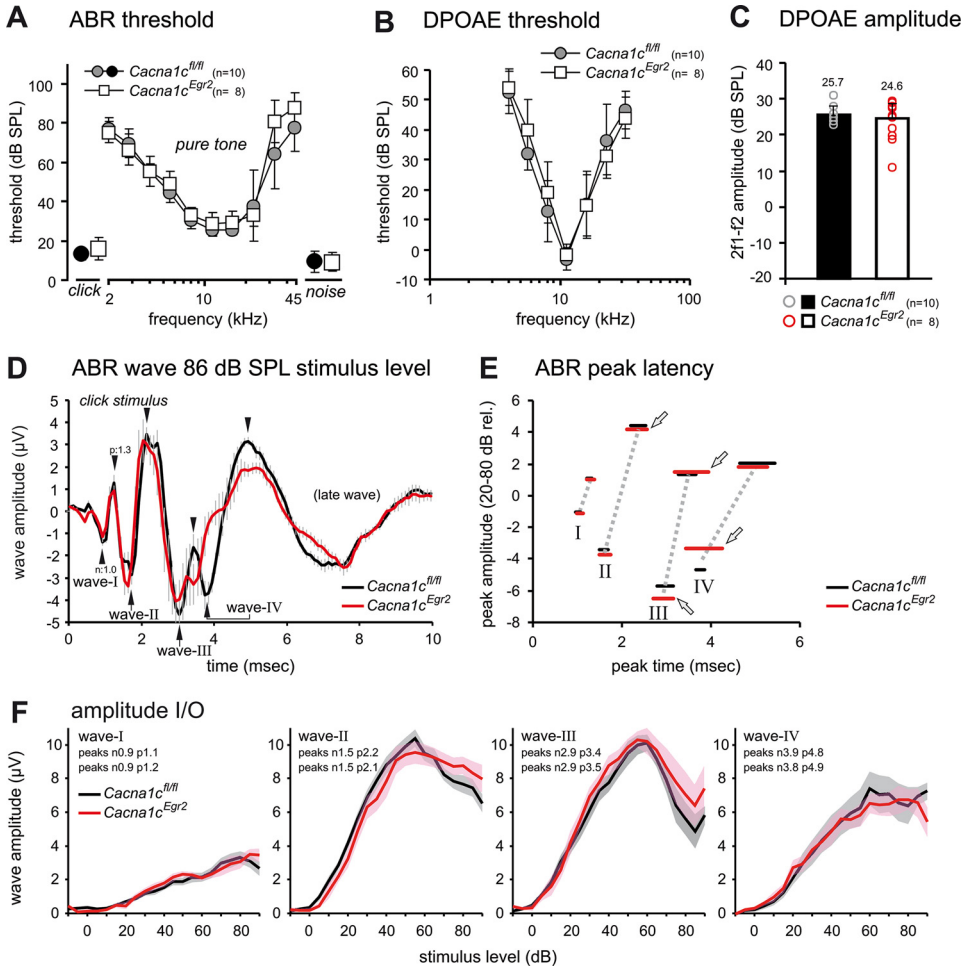

FIGURE 8. **Nearly normal ABRs in *Cacna1c*^{Egr2} mice.** *A*, ABR thresholds were invariant between *Cacna1c*$^{fl/fl}$ (control, *closed circles*) and *Cacna1c*^{Egr2} mice (*open squares*) for pure tone stimuli ($p > 0.05$, two-way analysis of variance), click stimuli (*lower left corner*), and noise burst stimuli (*lower right corner*). Mean values ± S.D. *B*, DPOAE thresholds for *Cacna1c*$^{fl/fl}$ (*closed circles*) and *Cacna1c*^{Egr2} mice (*open squares*) were not significantly different ($p > 0.05$, two-way analysis of variance). *C*, signal strength for the 2*f*1 − *f*2 distortion product at 50 db SPL *f*1 stimulation level was not significantly different for *Cacna1c*$^{fl/fl}$ (*closed bar*) and *Cacna1c*^{Egr2} mice (*open bar*, $p = 0.15$, one-sided *t* test). Emission signals of individual ears are shown as *circles* within each *bar*. *D*, click-evoked ABR waves (mean values ± S.E.) from *Cacna1c*$^{fl/fl}$ (*black*) and *Cacna1c*^{Egr2} (*red*) mice for an 86-db SPL stimulus were overlaid for comparison. The peaks corresponding to ABR wave I to wave IV are indicated. Waves are defined by their leading negative (*n*) and following positive (*p*) peak, as illustrated for wave I. ABR wave amplitudes and peak latencies differed between genotypes, and differences were most pronounced for waves II–IV. *E*, responsible for the changed ABR waveform in *D* was a larger variation of peak occurrence between 2 and 4 ms in individual *Cacna1c*^{Egr2} mice, as indicated by the larger horizontal extension of the bar (*arrows*, ±1 S.D. of the ABR peak latencies from individual ears for stimulus levels between 20 and 80 db). Peaks corresponding to associated waves are connected by *dashed lines*. *F*, normal peak amplitudes in *Cacna1c*^{Egr2} mice. Average I/O functions from control mice are shown as *black lines* and from *Cacna1c*^{Egr2} mice as *red lines* (±S.E.).

Analyses of Candidate Pathways for Increased Postnatal Death of SOC Neurons—The cAMP response element-binding protein (CREB) has been widely implicated in the survival of neurons and is activated by L-VGCCs (62–65). Of note, in the AVCN, deafferentation sharply increases the amount of phosphorylated CREB (p-CREB), likely triggering a pro-survival signaling cascade (66). To study whether the phosphorylation of CREB was also increased in auditory brainstem neurons lacking $Ca_v1.2$, we performed immunohistochemical analyses of p-CREB in the DCN, PVCN, AVCN, LSO, and MNTB at P0 and P4 (Fig. 10, shown for the MNTB). p-CREB displays a dynamic pattern during perinatal development, but no difference was observed between both genotypes (Fig. 10). The lack of any differences in p-CREB labeling between control and *Cacna1c*^{Egr2} mice argues against a role for this protein in the survival of $Ca_v1.2$-deprived auditory neurons. This conclusion is supported by the significant cell loss in the MNTB and DCN, despite considerable p-CREB expression.

A signaling cascade involved in deafferentation-associated cell death in the auditory brainstem involves NFATc4, the death receptor Fas, and its ligand, FasL. NFATc4 displayed an increased nuclear localization and FasL an increased expression in mice during deafferentation-induced cell death via immunohistochemistry and semiquantitative RT-PCR, respectively (67). To probe this pathway, we performed similar experiments. Immunohistochemical studies revealed no change in the subcellular localization of NFATc4 between *Cacna1c*^{Egr2} mice and control littermates (Fig. 11*A*, *i–iv*, shown for MNTB). Furthermore, quantitative RT-PCR experiments revealed no up-regulation of FasL or Fas in the P2 SOC (Fig. 11*B*, FasL, 1.06 ± 0.24-fold change; Fas, 1.17 ± 0.09-fold), suggesting that this signaling pathway does not underlie increased cell death in *Cacna1c*^{Egr2} mice.

We next focused on neurotrophins, as they play an important role in neuronal survival (68). Previous studies in the developing auditory brainstem reveal that BDNF and NT3 and their high-affinity tyrosine kinase receptors TrkB and TrkC start to

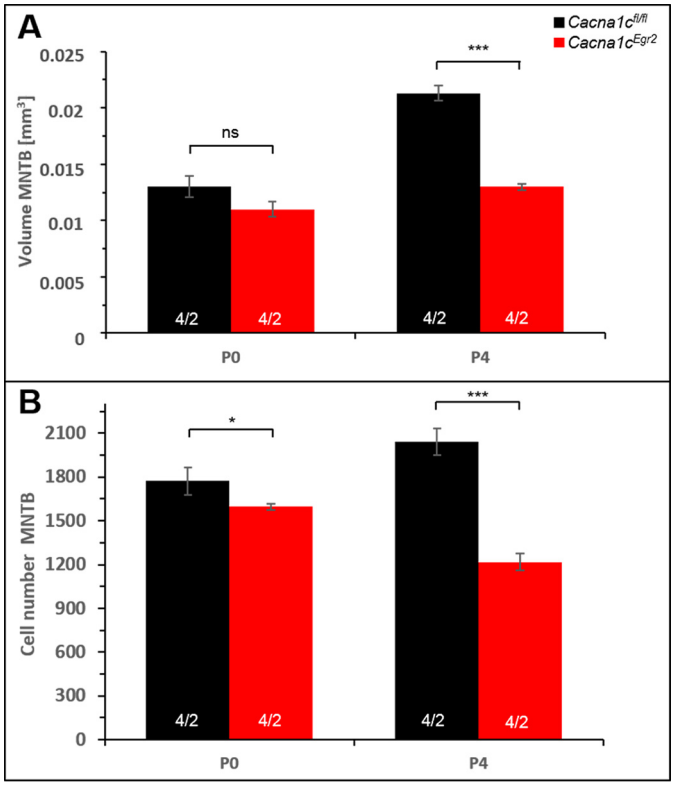

FIGURE 9. **Rapid postnatal loss of MNTB neurons in *Cacna1c*^{Egr2} mice.** Volume and cell number were determined at P0 (*A*) and P4 (*B*) from Nissl-stained serial sections (four nuclei from two animals). A highly significant decrease in volume and cell number was observed in *Cacna1c*^{Egr2} mice at P4 but not at P0. *Black*, control *Cacna1c*$^{fl/fl}$ mice; *red*, *Cacna1c*^{Egr2} mice. As a test for statistical significance, Student's *t* test was used. *, $p \leq 0.01$; ***, $p \leq 0.001$; *ns*, not significant.

be expressed from P3 onwards (69, 70). TrkA is not expressed at all (70). In contrast, p75NTR is expressed already in the perinatal auditory brainstem and present even at late embryonic stages (71). This makes p75NTR the most promising candidate for study, as it is present during the occurrence of cell death in *Cacna1c*^{Egr2} mice. Furthermore, in association with Sort1, this neurotrophin receptor promotes cell death (68). We focused on the SOC, as its nuclei exhibited the strongest cell loss. Immunohistochemical analysis of p75NTR and Sort1 showed no difference in abundance between *Cacna1c*^{Egr2} mice and control littermates (Fig. 11*A*, *v–viii* and *iv–xii*). This was confirmed on the mRNA level by quantitative RT-PCR analysis of P2 SOC tissue (Fig. 11*B*, -fold change p75NTR, 0.93 ± 0.11-fold change; -fold change Sort1, 0.89 ± 0.39-fold).

Finally, we analyzed the expression of Iba1, a marker for activated microglia (72). Microglia play an important role in controlled phagocytosis during development but are also highly activated during pathological cell loss, as shown for retinal degeneration (73) and neurodegenerative diseases (74). Quantitative immunohistochemical analysis demonstrated no change in the number of Iba1-positive cells in the P2 MNTB (Fig. 11*A*, *xiii* and *xiv*; Fig 11*C*, control, 5.83 ± 0.5; *Cacna1c*^{Egr2}, 4.58 ± 0.48). Together, these data imply the operation of other cell death-triggering pathways in *Cacna1c*^{Egr2} mice than observed after deafferentation. Alternatively, the lack of a precisely timed intervention, a hallmark of deafferentation protocols, might impair the detection of alterations in signaling cascades, which often are short-lived.

Discussion

Our study demonstrates that lack of $Ca_v1.2$ causes neuronal loss and volume reduction of auditory brainstem nuclei, similar to the defects seen when $Ca_v1.3$ is absent. Thus, $Ca_v1.2$ and $Ca_v1.3$ have a common function concerning the survival of auditory neurons. Nevertheless, each channel type cannot compensate the loss of its paralogous protein. In contrast to $Ca_v1.3$, the deletion of $Ca_v1.2$ narrows the spike width. However, absence of $Ca_v1.2$ does not appear to alter the other biophysical properties and basic aspects of synaptic transmission. In addition, it only marginally affects ABRs. We identified P0–P4 as the period in which a significant number of auditory brainstem neurons are lost in the absence of $Ca_v1.2$. Finally, we observed no differences in several signaling cascades associated with neuronal cell death in *Cacna1c*^{Egr2} mice.

The Role of Ca^{2+} in a Life-or-Death Decision in the Auditory Brainstem—Our study has established a critical role of $Ca_v1.2$ in maintaining the integrity of auditory brainstem centers. We observed a volume decrease between 11.9% (AVCN) and 35% (LSO) in *Cacna1c*^{Erg2} mice due to post-migratory cell death (Figs. 2 and 9). Hence, both neuronal L-VGCCs are required for auditory brainstem integrity, as *Cacna1d*$^{-/-}$ mice (33) and *Cacna1d*^{Egr2} mice (34) also showed significant volume decreases and neuronal loss. A role for both channel types in neuronal survival was also suggested for spiral ganglion neurons, based on histological analyses of 2- and 4-month-old *Cacna1d*$^{-/-}$ or heterozygous *Cacna1c*$^{+/-}$ mice (75). Of note, auditory neurons show a bimodal reaction upon disturbed synaptic signaling, as part of the auditory brainstem neurons is able to survive, whereas a significant number undergo cell death (76). This is in agreement with previous reports on deafferented auditory neurons (77, 78). Indeed, the first report dates back to 1949, when Levi-Montalcini (79) described significant neuronal loss in auditory brainstem structures upon otocyst extirpation in the chick embryo.

The *in vivo* signaling pathways involved in the survival of auditory neurons have remained largely unknown. Our data demonstrate for the first time *in vivo* that L-VGCC-mediated Ca^{2+} signaling is required for the postmigratory integrity of auditory nuclei. A comparison of our data with previous studies, however, indicates an ambivalent role for Ca^{2+} signaling. In the AVCN of cochlea-deprived animals, cell death is triggered by a hypercalcemic condition caused by an increased Ca^{2+} influx through AMPA receptors (66, 67, 76), likely potentiated by L-VGCCs (76, 80). Our results in *Cacna1c*- or *Cacna1d*-deficient mice demonstrate the *in vivo* importance of Ca^{2+} entry via L-VGCCs as a survival-promoting signal (this study and Ref. 33, 34). These partially opposing findings may be reconciled by the fact that auditory brainstem neurons appear to be very sensitive to the optimal range of Ca^{2+} influx (30, 81). The survival of rat SOC slice cultures depended on depolarization by 25 mM K^+ in the medium in order to open L-VGCCs, whereas 40 mM K^+ was detrimental. This demonstrates a narrow window for pro-survival Ca^{2+} signaling in auditory neurons, in agreement with results obtained in other neuronal sys-

TABLE 5
Quantification of structural changes in the MNTB of neonatal *Cacna1c*$^{fl/fl}$ and *Cacna1c*^{Egr2} mice
Values are means ± S.D.

	Volume				Cell number			
	Cacna1c$^{fl/fl}$	*Cacna1c*^{Egr2}	*p* value	% reduction	*Cacna1c*$^{fl/fl}$	*Cacna1c*^{Egr2}	*p* value	% reduction
P0 MNTB	0.013 ± 0.0009	0.011 ± 0.0007	0.241	15.4%	1771 ± 94	1596 ± 23	0.041	9.9%
P4 MNTB	0.021 ± 0.0006	0.013 ± 0.0002	0.0000001	39.0%	2041 ± 91	1217 ± 59	0.000005	40.4%

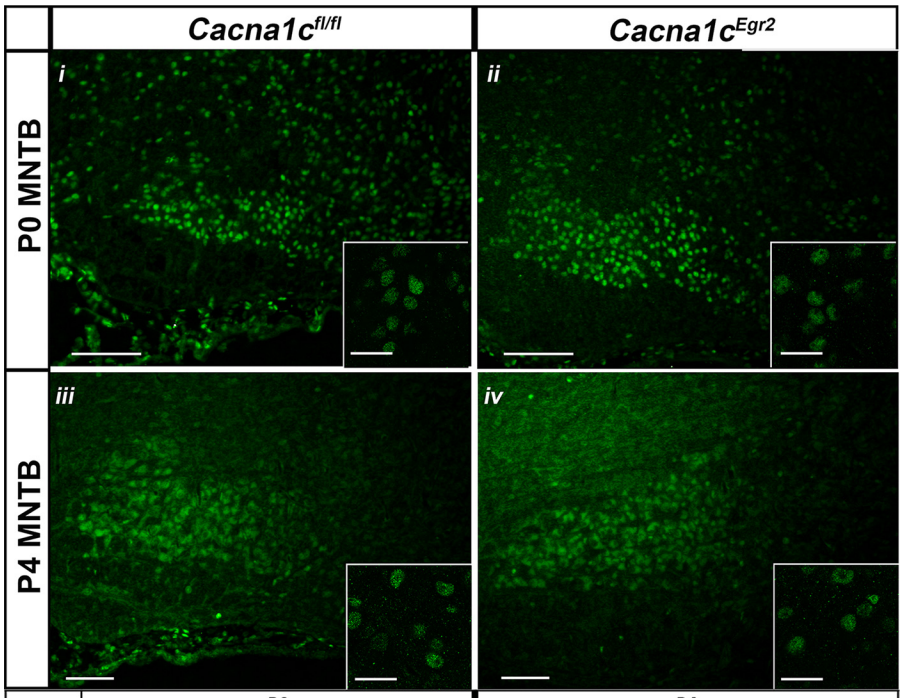

	P0		P4	
	Cacna1c$^{fl/fl}$	*Cacna1c*^{Egr2}	*Cacna1c*$^{fl/fl}$	*Cacna1c*^{Egr2}
DCN	o	o	o	o
PVCN	o	o	-	-
AVCN	+	+	o	o
LSO	o	o	-	-
MNTB	+	+	+	+

FIGURE 10. **No change in p-CREB immunoreactivity in *Cacna1c*^{Egr2} mice.** Shown is the immunohistochemistry of p-CREB in the MNTB of control (*i* and *iii*) and *Cacna1c*^{Egr2} mice (*ii* and *iv*) at P0 and P4. The labeling intensity of the other auditory nuclei is documented in the *lower panel*. At P0, strong p-CREB immunoreactivity was observed in the AVCN and MNTB, whereas the DCN, PVCN, and LSO were moderately labeled. At P4, strong labeling persisted in the MNTB and moderate labeling in the DCN, whereas the AVCN, PVCN, and the LSO showed decreased p-CREB immunoreactivity. No differences were observed between control and *Cacna1c*^{Egr2} mice. Dorsal is *up*, and lateral is to the *right*. *Scale bars*, 100 μm; for *inserts*, 20 μm.

tems (82, 83). The importance of the intracellular Ca^{2+} homeostasis is supported by the developmentally regulated expression pattern of the Ca^{2+}-buffering proteins calbindin, calretinin, and parvalbumin in the auditory brainstem (84, 85) and changes therein upon altered neuronal activity (86).

Downstream Signaling of L-VGGCs—Deafferentation studies have linked cell survival in auditory brainstem nuclei to the transcription factor p-CREB (66) and cell death to NFAT4c signaling (67). Our immunohistochemical analysis of either of these pathways revealed no difference between control and *Cacna1c*^{Erg2} mice (Figs. 10 and 11). Two explanations may account for this discrepancy. Deafferentation represents an unnatural condition that might trigger both physiological and nonphysiological responses. Secondly, deafferentation provides a precise time point, and the reported alterations in p-CREB and NFATc4 were observed only during a narrow time window of about 1 h. Such a sharp window for the majority of neurons might not be present in *Cacna1c*^{Erg2} mice, as the trigger for the respective signaling cascade likely shows a high intercellular variety. The time period of the altered signaling pathways might be, for instance, a function of the precise time of innervation during development, which differs for individual neurons.

Alternatively, disrupted BDNF signaling was proposed to cause the cell death of deafferented MNTB neurons (77). Of note, L-VGCC-mediated signaling has been tightly linked to BDNF expression (87–89). However, BDNF (69) and its major receptor TrkB (70) are barely expressed at P0 throughout the auditory brainstem, and their expression increases up to P15, implying a role during the maturation of auditory neurons. Similar results have been obtained for NTF3, NTF4, and TrkC (70, 69). We therefore focused on p75NTR and Sort1, as both together can promote cell death. Both on the mRNA and protein level, no difference between the two genotypes was

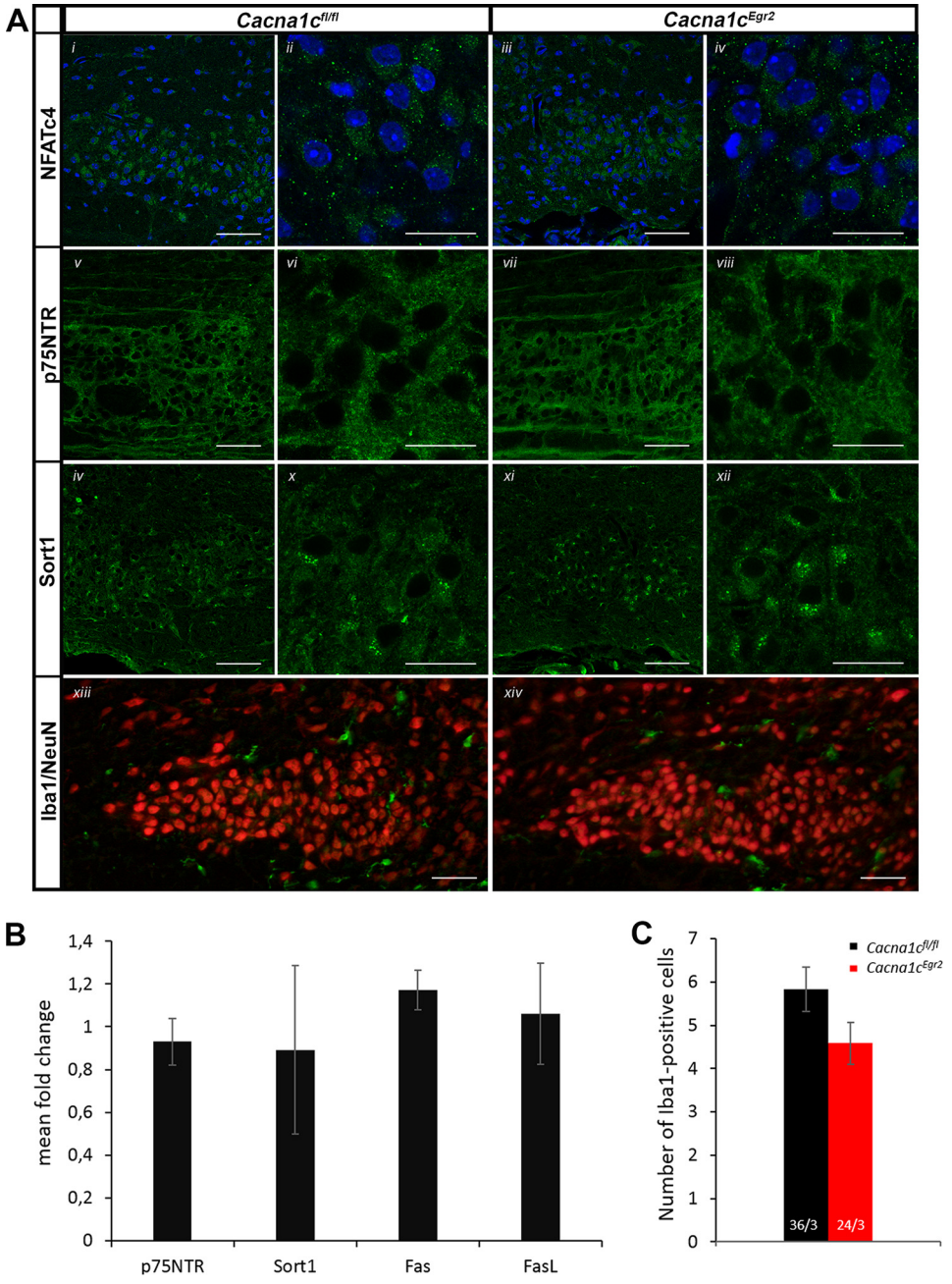

FIGURE 11. **No changes in signaling pathways associated with cell death in *Cacna1c*^{Egr2} mice at P2.** *A*, immunohistochemistry of NFATc4 (*i–iv*; *green* = NFATc4, *blue* = TO-PRO-3), p75NTR (*v–viii*), Sort1 (*iv–xii*), and Iba1 (*xiii* and *xiv*; *green* = Iba1, *red* = NeuN) in the MNTB of control (*i/ii*, *v/vi*, *iv/x*, and *xiii*) and *Cacna1c*^{Egr2} mice (*iii/iv*, *vii/viii*, *xi/xii*, and *xiv*). For all investigated proteins there was no difference in the staining pattern, subcellular localization, or intensity between the two genotypes. Dorsal is *up*, and lateral is to the *right*. *Scale bars*, 50 μm (*i*, *iii*, *v*, *vii*, *iv*, *xi*, *xiii*, and *xiv*) and 20 μm (*ii*, *iv*, *vi*, *viii*, *x*, and *xii*). *B*, mean fold change ± S.E. in gene expression revealed by qRT-PCR for p75NTR, Sort1, Fas, and FasL. No significant up- or down-regulation of these gene products was observed in *Cacna1c*^{Egr2} mice. *C*, quantification of Iba1-positive cells in the MNTB of *Cacna1c*$^{fl/fl}$ and *Cacna1c*^{Egr2} mice (mean ± S.E.). Analysis of 36 MNTB slices of three *Cacna1c*^{Egr2} mice and 24 MNTB slices of three control mice revealed no difference in the number of Iba1-positive cells. Student's *t* test was used to test for statistical significance.

observed, arguing against a role for this pathway in the observed cell death. Yet, it is not excluded that lack of $Ca_v1.2$ causes the release of proneurotrophins, which then activate p75NTR-coupled apoptotic pathways. It might therefore still be worthwhile to cross *Cacna1c*^{Erg2} mice with available p75NTR null mice (90).

Circuit Formation and Neonatal Cell Loss—Our anatomical analysis revealed a considerable decline in the number of MNTB neurons between P0 and P4 in *Cacna1c*^{Erg2} mice, which corresponds well with the time period observed in *Atoh1*^{Erg2} mice (91). In these animals, the number of MNTB neurons decreases to 50% of the control value by P3 and to 30% by P7, with no further decline thereafter. Developing MNTB neurons become functionally innervated in the mouse at embryonic day 17 (E17), immediately after migration and ~2 days prior to birth (92). In addition, spontaneous EPSCs can be recorded from MNTB neurons at E17, in agreement with spontaneous activity originating in the cochlea prior to hearing onset (59, 60). Taken together, our data identify a neonatal period directly after functional circuit formation, during which auditory brain-

stem neurons appear to depend on synaptic signaling involving L-VGCCs. Of note, inhibitory neurotransmitters cause depolarization of auditory neurons during this perinatal period (93–96), enabling "inhibitory" projections to execute pro-survival signaling through L-VGCCs. The precise closing of this period of vulnerability, however, has yet to be determined. Experiments in gerbils demonstrate a sharp border between P7 and P9 with respect to survival of AVCN neurons following deafferentation (97).

Different Impact of $Ca_v1.2$ and $Ca_v1.3$ Signaling on Biophysical Properties of Auditory Brainstem Neurons—Lack of $Ca_v1.2$ affects spike shape in an opposite way than lack of $Ca_v1.3$. Whereas LSO neurons of *Cacna1c*^{Egr2} mice exhibit a 17% narrower half-width, spikes are wider by 40% in *Cacna1d* knock-out mice (33). To investigate the underlying mechanism, we examined the expression of BK channels. However, immunohistochemistry revealed no quantitative or qualitative differences between the two genotypes (Fig. 5). The sparse expression of Kcnma1 further argues against a major contribution of BK channels to the spike shape of LSO neurons. Therefore, additional studies will be needed to investigate the underlying mechanism of narrower action potentials in these mice, which will likely involve altered expression of voltage-gated Na^+ or K^+ channels (98).

Notable are the many unchanged electrophysiological properties of surviving neurons in *Cacna1c*^{Egr2} mice. Apparently, $Ca_v1.2$ is required mainly for cell survival, or compensatory mechanisms enable nearly normal development of those neurons that survive.

Another notable difference between *Cacna1c*^{Egr2} and *Cacna1d*^{Egr2} mice is demonstrated by the ABRs. *Cacna1d*^{Egr2} animals display a higher excitation in auditory brainstem nuclei, whereas ABR thresholds and amplitudes are nearly normal in *Cacna1c*^{Egr2} mice (Fig. 8). As a corollary, these nearly normal ABRs in mice with reduced volumes of the auditory brainstem nuclei (up to 35%) illustrate that ABR amplitudes do not mirror such brainstem abnormalities. In concordance with the difference in ABRs of *Cacna1c*^{Egr2}and *Cacna1d*^{Egr2} mice is the altered spiking behavior of LSO neurons in *Cacna1d*^{Egr2}, which was not observed in *Cacna1c*^{Egr2}animals. Whereas the majority of $Ca_v1.2$-deficient LSO neurons fire a single action potential, most $Ca_v1.3$-deficient neurons fire multiple times.

The stronger auditory phenotype in *Cacna1d*^{Egr2}mice compared with *Cacna1c*^{Egr2} mice might be attributed to a stronger contribution of the $Ca_v1.3$ channels (30%) to a total Ca^{2+} influx in perinatal LSO neurons compared with $Ca_v1.2$ (6%) (36). Furthermore, $Ca_v1.3$ channels open at more negative membrane potentials than $Ca_v1.2$ channels (99, 100). In postsynaptic neurons, this may trigger Ca^{2+} influx more readily during the period of spontaneous activity. Moreover, this Ca^{2+} influx and the associated depolarization may facilitate the opening of $Ca_v1.2$ channels. If so, *Cacna1d*^{Egr2} mice suffer not only from a lack of Ca^{2+} entry through $Ca_v1.3$ channels but also from impaired opening of $Ca_v1.2$ channels.

Finally, the more severe central auditory phenotype in $Ca_v1.3$ knock-out mice, together with a pivotal role for this channel at the inner hair cell synapses, reveals an intriguing recruitment of this channel to the auditory system during evolution (101). This is in contrast to most other brain areas, where $Ca_v1.2$ is the predominant form (3).

In conclusion, our data demonstrate overlapping as well as distinct functions for $Ca_v1.2$ and $Ca_v1.3$ in the developing auditory brainstem. Despite their co-expression in auditory neurons, both channel types are required for neuronal survival and cannot substitute for one another. This is also indicated by their differing impact on the signal processing and firing behavior of auditory neurons.

Author Contributions—H. G. N. conceived and coordinated the study. L. E. designed, performed, and analyzed the experiments shown in Figs. 1, 2, 5, 10, and 11. S. V. S. initiated the analysis of the mouse model, contributed to Fig. 2, and performed and analyzed the experiment shown in Fig. 9. E. F. designed the experiments in Figs. 4, 6, and 7, which were performed by K. J. with the help of D. G. L. R. and M. K. designed, performed, and analyzed the experiments shown in Fig. 8. M. B. and M. M. designed, performed, and analyzed the experiments shown in Fig. 3. Finally, F. H. contributed the floxed mice. All authors reviewed the results and approved the final version of the manuscript.

Acknowledgments—We thank Anja Feistner, Moritz Stöcklin, and Martina Reents for excellent technical assistance and Nele Griepenstroh for help with the RT-qPCR experiments.

References

1. Catterall, W. A. (2011) Voltage-gated calcium channels. *Cold Spring Harb. Perspect. Biol.* **3,** a003947
2. Dolphin, A. C. (2009) Calcium channel diversity: multiple roles of calcium channel subunits. *Curr. Opin. Neurobiol.* **19,** 237–244
3. Sinnegger-Brauns, M. J., Huber, I. G., Koschak, A., Wild, C., Obermair, G. J., Einzinger, U., Hoda, J. C., Sartori, S. B., and Striessnig, J. (2009) Expression and 1,4-dihydropyridine-binding properties of brain L-type calcium channel isoforms. *Mol. Pharmacol.* **75,** 407–414
4. Galli, C., Meucci, O., Scorziello, A., Werge, T. M., Calissano, P., and Schettini, G. (1995) Apoptosis in cerebellar granule cells is blocked by high KCl, forskolin, and IGF-1 through distinct mechanisms of action: the involvement of intracellular calcium and RNA synthesis. *J. Neurosci.* **15,** 1172–1179
5. Heck, N., Golbs, A., Riedemann, T., Sun, J. J., Lessmann, V., and Luhmann, H. J. (2008) Activity-dependent regulation of neuronal apoptosis in neonatal mouse cerebral cortex. *Cereb. Cortex* **18,** 1335–1349
6. Chernyshova, Y., Leshchyns'ka, I., Hsu, S. C., Schachner, M., and Sytnyk, V. (2011) The neural cell adhesion molecule promotes FGFR-dependent phosphorylation and membrane targeting of the exocyst complex to induce exocytosis in growth cones. *J. Neurosci.* **31,** 3522–3535
7. Enslen, H., and Soderling, T. R. (1994) Roles of calmodulin-dependent protein kinases and phosphatase in calcium-dependent transcription of immediate early genes. *J. Biol. Chem.* **269,** 20872–20877
8. Porcher, C., Hatchett, C., Longbottom, R. E., McAinch, K., Sihra, T. S., Moss, S. J., Thomson, A. M., and Jovanovic, J. N. (2011) Positive feedback regulation between γ-aminobutyric acid type A (GABA(A)) receptor signaling and brain-derived neurotrophic factor (BDNF) release in developing neurons. *J. Biol. Chem.* **286,** 21667–21677
9. Zucca, S., and Valenzuela, C. F. (2010) Low concentrations of alcohol inhibit BDNF-dependent GABAergic plasticity via L-type Ca2+ channel inhibition in developing CA3 hippocampal pyramidal neurons. *J. Neurosci.* **30,** 6776–6781
10. Grubb, M. S., and Burrone, J. (2010) Activity-dependent relocation of the axon initial segment fine-tunes neuronal excitability. *Nature* **465,** 1070–1074
11. Fulton, D., Paez, P. M., Fisher, R., Handley, V., Colwell, C. S., and Campagnoni, A. T. (2010) Regulation of L-type Ca++ currents and process

morphology in white matter oligodendrocyte precursor cells by golli-myelin proteins. *Glia* **58,** 1292–1303
12. Wankerl, K., Weise, D., Gentner, R., Rumpf, J. J., and Classen, J. (2010) L-type voltage-gated Ca2+ channels: a single molecular switch for long-term potentiation/long-term depression-like plasticity and activity-dependent metaplasticity in humans. *J. Neurosci.* **30,** 6197–6204
13. Schierberl, K., Giordano, T., Satpute, S., Hao, J., Kaur, G., Hofmann, F., Moosmang, S., Striessnig, J., and Rajadhyaksha, A. (2012) Cav 1.3 L-type Ca (2+) channels mediate long-term adaptation in dopamine D2L-mediated GluA1 trafficking in the dorsal striatum following cocaine exposure. *Channels* (*Austin*) **6,** 11–17
14. Schierberl, K., Hao, J., Tropea, T. F., Ra, S., Giordano, T. P., Xu, Q., Garraway, S. M., Hofmann, F., Moosmang, S., Striessnig, J., Inturrisi, C. E., and Rajadhyaksha, A. M. (2011) Cav1.2 L-type Ca(2)(+) channels mediate cocaine-induced GluA1 trafficking in the nucleus accumbens, a long-term adaptation dependent on ventral tegmental area Ca(v)1.3 channels. *J. Neurosci.* **31,** 13562–13575
15. Zuccotti, A., Clementi, S., Reinbothe, T., Torrente, A., Vandael, D. H., and Pirone, A. (2011) Structural and functional differences between L-type calcium channels: crucial issues for future selective targeting. *Trends Pharmacol. Sci.* **32,** 366–375
16. Berger, S. M., and Bartsch, D. (2014) The role of L-type voltage-gated calcium channels Ca1.2 and Ca 1.3 in normal and pathological brain function. *Cell Tissue Res.* **357,** 463–476
17. Splawski, I., Timothy, K. W., Sharpe, L. M., Decher, N., Kumar, P., Bloise, R., Napolitano, C., Schwartz, P. J., Joseph, R. M., Condouris, K., Tager-Flusberg, H., Priori, S. G., Sanguinetti, M. C., and Keating, M. T. (2004) Ca(V)1.2 calcium channel dysfunction causes a multisystem disorder including arrhythmia and autism. *Cell* **119,** 19–31
18. Antzelevitch, C., Pollevick, G. D., Cordeiro, J. M., Casis, O., Sanguinetti, M. C., Aizawa, Y., Guerchicoff, A., Pfeiffer, R., Oliva, A., Wollnik, B., Gelber, P., Bonaros, E. P., Jr., Burashnikov, E., Wu, Y., Sargent, J. D., Schickel, S., Oberheiden, R., Bhatia, A., Hsu, L. F., Haïssaguerre, M., Schimpf, R., Borggrefe, M., and Wolpert, C. (2007) Loss-of-function mutations in the cardiac calcium channel underlie a new clinical entity characterized by ST-segment elevation, short QT intervals, and sudden cardiac death. *Circulation* **115,** 442–449
19. Napolitano, C., and Antzelevitch, C. (2011) Phenotypical manifestations of mutations in the genes encoding subunits of the cardiac voltage-dependent L-type calcium channel. *Circ. Res.* **108,** 607–618
20. Purcell, S. M., Moran, J. L., Fromer, M., Ruderfer, D., Solovieff, N., Roussos, P., O'Dushlaine, C., Chambert, K., Bergen, S. E., Kähler, A., Duncan, L., Stahl, E., Genovese, G., Fernández, E., Collins, M. O., Komiyama, N. H., Choudhary, J. S., Magnusson, P. K., Banks, E., Shakir, K., Garimella, K., Fennell, T., DePristo, M., Grant, S. G., Haggarty, S. J., Gabriel, S., Scolnick, E. M., Lander, E. S., Hultman, C. M., Sullivan, P. F., McCarroll, S. A., and Sklar, P. (2014) A polygenic burden of rare disruptive mutations in schizophrenia. *Nature* **506,** 185–190
21. Ripke, S., O'Dushlaine, C., Chambert, K., Moran, J. L., Kähler, A. K., Akterin, S., Bergen, S. E., Collins, A. L., Crowley, J. J., Fromer, M., Kim, Y., Lee, S. H., Magnusson, P. K., Sanchez, N., Stahl, E. A., Williams, S., Wray, N. R., Xia, K., Bettella, F., Borglum, A. D., Bulik-Sullivan, B. K., Cormican, P., Craddock, N., de Leeuw, C., Durmishi, N., Gill, M., Golimbet, V., Hamshere, M. L., Holmans, P., Hougaard, D. M., Kendler, K. S., Lin, K., Morris, D. W., Mors, O., Mortensen, P. B., Neale, B. M., O'Neill, F. A., Owen, M. J., Milovancevic, M. P., Posthuma, D., Powell, J., Richards, A. L., Riley, B. P., Ruderfer, D., Rujescu, D., Sigurdsson, E., Silagadze, T., Smit, A. B., Stefansson, H., Steinberg, S., Suvisaari, J., Tosato, S., Verhage, M., Walters, J. T., Levinson, D. F., Gejman, P. V., Laurent, C., Mowry, B. J., O'Donovan, M. C., Pulver, A. E., Schwab, S. G., Wildenauer, D. B., Dudbridge, F., Shi, J., Albus, M., Alexander, M., Campion, D., Cohen, D., Dikeos, D., Duan, J., Eichhammer, P., Godard, S., Hansen, M., Lerer, F. B., Liang, K. Y., Maier, W., Mallet, J., Nertney, D. A., Nestadt, G., Norton, N., Papadimitriou, G. N., Ribble, R., Sanders, A. R., Silverman, J. M., Walsh, D., Williams, N. M., Wormley, B., Arranz, M. J., Bakker, S., Bender, S., Bramon, E., Collier, D., Crespo-Facorro, B., Hall, J., Iyegbe, C., Jablensky, A., Kahn, R. S., Kalaydjieva, L., Lawrie, S., Lewis, C. M., Linszen, D. H., Mata, I., McIntosh, A., Murray, R. M., Ophoff, R. A., van Os, J., Walshe, M., Weisbrod, M., Wiersma, D., Donnelly, P., Barroso, I., Blackwell, J. M., Brown, M. A., Casas, J. P., Corvin, A. P., Deloukas, P., Duncanson, A., Jankowski, J., Markus, H. S., Mathew, C. G., Palmer, Colin N A, Plomin, R., Rautanen, A., Sawcer, S. J., Trembath, R. C., Viswanathan, A. C., Wood, N. W., Spencer, Chris C A, Band, G., Bellenguez, C., Freeman, C., Hellenthal, G., Giannoulatou, E., Pirinen, M., Pearson, R. D., Strange, A., Su, Z., Vukcevic, D., Langford, C., Hunt, S. E., Edkins, S., Gwilliam, R., Blackburn, H., Bumpstead, S. J., Dronov, S., Gillman, M., Gray, E., Hammond, N., Jayakumar, A., McCann, O. T., Liddle, J., Potter, S. C., Ravindrarajah, R., Ricketts, M., Tashakkori-Ghanbaria, A., Waller, M. J., Weston, P., Widaa, S., Whittaker, P., McCarthy, M. I., Stefansson, K., Scolnick, E., Purcell, S., McCarroll, S. A., Sklar, P., Hultman, C. M., and Sullivan, P. F. (2013) Genome-wide association analysis identifies 13 new risk loci for schizophrenia. *Nat. Genet.* **45,** 1150–1159
22. Yoshimizu, T., Pan, J. Q., Mungenast, A. E., Madison, J. M., Su, S., Ketterman, J., Ongur, D., McPhie, D., Cohen, B., Perlis, R., and Tsai, L. H. (2015) Functional implications of a psychiatric risk variant within CACNA1C in induced human neurons. *Mol. Psychiatry* **20,** 284
23. Seisenberger, C., Specht, V., Welling, A., Platzer, J., Pfeifer, A., Kühbandner, S., Striessnig, J., Klugbauer, N., Feil, R., and Hofmann, F. (2000) Functional embryonic cardiomyocytes after disruption of the L-type α1C (Cav1.2) calcium channel gene in the mouse. *J. Biol. Chem.* **275,** 39193–39199
24. Moosmang, S., Haider, N., Klugbauer, N., Adelsberger, H., Langwieser, N., Müller, J., Stiess, M., Marais, E., Schulla, V., Lacinova, L., Goebbels, S., Nave, K. A., Storm, D. R., Hofmann, F., and Kleppisch, T. (2005) Role of hippocampal Cav1.2 Ca2+ channels in NMDA receptor-independent synaptic plasticity and spatial memory. *J. Neurosci.* **25,** 9883–9892
25. Baig, S. M., Koschak, A., Lieb, A., Gebhart, M., Dafinger, C., Nürnberg, G., Ali, A., Ahmad, I., Sinnegger-Brauns, M. J., Brandt, N., Engel, J., Mangoni, M. E., Farooq, M., Khan, H. U., Nürnberg, P., Striessnig, J., and Bolz, H. J. (2011) Loss of Ca (v) 1.3 (CACNA1D) function in a human channelopathy with bradycardia and congenital deafness. *Nat. Neurosci.* **14,** 77–84
26. Platzer, J., Engel, J., Schrott-Fischer, A., Stephan, K., Bova, S., Chen, H., Zheng, H., and Striessnig, J. (2000) Congenital deafness and sinoatrial node dysfunction in mice lacking class D L-type Ca2+ channels. *Cell* **102,** 89–97
27. McKinney, B. C., and Murphy, G. G. (2006) The L-type voltage-gated calcium channel Cav1.3 mediates consolidation, but not extinction, of contextually conditioned fear in mice. *Learn. Mem.* **13,** 584–589
28. Pinggera, A., Lieb, A., Benedetti, B., Lampert, M., Monteleone, S., Liedl, K. R., Tuluc, P., and Striessnig, J. (2015) CACNA1D *de novo* mutations in autism spectrum disorders activate Cav1.3 L-type calcium channels. *Biol. Psychiatry* **77,** 816–822
29. Scholl, U. I., Goh, G., Stölting, G., de Oliveira, R. C., Choi, M., Overton, J. D., Fonseca, A. L., Korah, R., Starker, L. F., Kunstman, J. W., Prasad, M. L., Hartung, E. A., Mauras, N., Benson, M. R., Brady, T., Shapiro, J. R., Loring, E., Nelson-Williams, C., Libutti, S. K., Mane, S., Hellman, P., Westin, G., Åkerström, G., Björklund, P., Carling, T., Fahlke, C., Hidalgo, P., and Lifton, R. P. (2013) Somatic and germline CACNA1D calcium channel mutations in aldosterone-producing adenomas and primary aldosteronism. *Nat. Genet.* **45,** 1050–1054
30. Lohmann, C., Ilic, V., and Friauf, E. (1998) Development of a topographically organized auditory network in slice culture is calcium dependent. *J. Neurobiol.* **34,** 97–112
31. Mao, Z., Bonni, A., Xia, F., Nadal-Vicens, M., and Greenberg, M. E. (1999) Neuronal activity-dependent cell survival mediated by transcription factor MEF2. *Science* **286,** 785–790
32. Marshall, J., Dolan, B. M., Garcia, E. P., Sathe, S., Tang, X., Mao, Z., and Blair, L. A. (2003) Calcium channel and NMDA receptor activities differentially regulate nuclear C/EBPβ levels to control neuronal survival. *Neuron* **39,** 625–639
33. Hirtz, J. J., Boesen, M., Braun, N., Deitmer, J. W., Kramer, F., Lohr, C., Müller, B., Nothwang, H. G., Striessnig, J., Löhrke, S., and Friauf, E. (2011) Cav1.3 calcium channels are required for normal development of the auditory brainstem. *J. Neurosci.* **31,** 8280–8294
34. Satheesh, S. V., Kunert, K., Rüttiger, L., Zuccotti, A., Schönig, K., Friauf,

E., Knipper, M., Bartsch, D., and Nothwang, H. G. (2012) Retrocochlear function of the peripheral deafness gene *Cacna1d*. *Hum. Mol. Genet.* **21,** 3896–3909
35. Hirtz, J. J., Braun, N., Griesemer, D., Hannes, C., Janz, K., Löhrke, S., Müller, B., and Friauf, E. (2012) Synaptic refinement of an inhibitory topographic map in the auditory brainstem requires functional Cav1.3 calcium channels. *J. Neurosci.* **32,** 14602–14616
36. Jurkovičová-Tarabová, B., Griesemer, D., Pirone, A., Sinnegger-Brauns, M. J., Striessnig, J., and Friauf, E. (2012) Repertoire of high voltage-activated calcium channels in lateral superior olive: functional analysis in wild-type, Cav1.3$^{-/-}$, and Cav1.2DHP$^{-/-}$ mice. *J. Neurophysiol.* **108,** 365–379
37. Voiculescu, O., Charnay, P., and Schneider-Maunoury, S. (2000) Expression pattern of a Krox-20/*Cre* knock-in allele in the developing hindbrain, bones, and peripheral nervous system. *Genesis* **26,** 123–126
38. Blaesse, P., Ehrhardt, S., Friauf, E., and Nothwang, H. G. (2005) Developmental pattern of three vesicular glutamate transporters in the rat superior olivary complex. *Cell Tissue Res.* **320,** 33–50
39. Ehmann, H., Salzig, C., Lang, P., Friauf, E., and Nothwang, H. G. (2008) Minimal sex differences in gene expression in the rat superior olivary complex. *Hear. Res.* **245,** 65–72
40. Pfaffl, M. W. (2001) A new mathematical model for relative quantification in real-time RT-PCR. *Nucleic Acids Res.* **29,** e45
41. Blosa, M., Sonntag, M., Brückner, G., Jäger, C., Seeger, G., Matthews, R. T., Rübsamen, R., Arendt, T., and Morawski, M. (2013) Unique features of extracellular matrix in the mouse medial nucleus of trapezoid body: implications for physiological functions. *Neuroscience* **228,** 215–234
42. Jäger, C., Lendvai, D., Seeger, G., Brückner, G., Matthews, R. T., Arendt, T., Alpár, A., and Morawski, M. (2013) Perineuronal and perisynaptic extracellular matrix in the human spinal cord. *Neuroscience* **238,** 168–184
43. Sterenborg, J. C., Pilati, N., Sheridan, C. J., Uchitel, O. D., Forsythe, I. D., and Barnes-Davies, M. (2010) Lateral olivocochlear (LOC) neurons of the mouse LSO receive excitatory and inhibitory synaptic inputs with slower kinetics than LSO principal neurons. *Hear. Res.* **270,** 119–126
44. Zuccotti, A., Lee, S. C., Campanelli, D., Singer, W., Satheesh, S. V., Patriarchi, T., Geisler, H. S., Köpschall, I., Rohbock, K., Nothwang, H. G., Hu, J., Hell, J. W., Schimmang, T., Rüttiger, L., and Knipper, M. (2013) L-type CaV1.2 deletion in the cochlea but not in the brainstem reduces noise vulnerability: implication for CaV1.2-mediated control of cochlear BDNF expression. *Front. Mol. Neurosci.* **6,** 20
45. Zhou, J., Nannapaneni, N., and Shore, S. (2007) Vesicular glutamate transporters 1 and 2 are differentially associated with auditory nerve and spinal trigeminal inputs to the cochlear nucleus. *J. Comp. Neurol.* **500,** 777–787
46. Rosengauer, E., Hartwich, H., Hartmann, A. M., Rudnicki, A., Satheesh, S. V., Avraham, K. B., and Nothwang, H. G. (2012) *Egr2::Cre*-mediated conditional ablation of Dicer disrupts histogenesis of mammalian ventral auditory nuclei. *PLoS ONE* **7,** e49503
47. Farago, A. F., Awatramani, R. B., and Dymecki, S. M. (2006) Assembly of the brainstem cochlear nuclear complex is revealed by intersectional and subtractive genetic fate maps. *Neuron* **50,** 205–218
48. Ehmann, H., Hartwich, H., Salzig, C., Hartmann, N., Clément-Ziza, M., Ushakov, K., Avraham, K. B., Bininda-Emonds, O. R., Hartmann, A. K., Lang, P., Friauf, E., and Nothwang, H. G. (2013) Time-dependent gene expression analysis of the developing superior olivary complex. *J. Biol. Chem.* **288,** 25865–25879
49. Xiao, L., Michalski, N., Kronander, E., Gjoni, E., Genoud, C., Knott, G., and Schneggenburger, R. (2013) BMP signaling specifies the development of a large and fast CNS synapse. *Nat. Neurosci.* **16,** 856–864
50. Maroto, M., Fernández-Morales, J. C., Padín, J. F., González, J. C., Hernández-Guijo, J. M., Montell, E., Vergés, J., de Diego, A. M., and García, A. G. (2013) Chondroitin sulfate, a major component of the perineuronal net, elicits inward currents, cell depolarization, and calcium transients by acting on AMPA and kainate receptors of hippocampal neurons. *J. Neurochem.* **125,** 205–213
51. Hrabetová, S., Masri, D., Tao, L., Xiao, F., and Nicholson, C. (2009) Calcium diffusion enhanced after cleavage of negatively charged components of brain extracellular matrix by chondroitinase ABC. *J. Physiol.* **587,** 4029–4049
52. Vigetti, D., Andrini, O., Clerici, M., Negrini, D., Passi, A., and Moriondo, A. (2008) Chondroitin sulfates act as extracellular gating modifiers on voltage-dependent ion channels. *Cell. Physiol. Biochem.* **22,** 137–146
53. Brückner, G., and Grosche, J. (2001) Perineuronal nets show intrinsic patterns of extracellular matrix differentiation in organotypic slice cultures. *Exp. Brain Res.* **137,** 83–93
54. Sausbier, U., Sausbier, M., Sailer, C. A., Arntz, C., Knaus, H. G., Neuhuber, W., and Ruth, P. (2006) Ca2+ -activated K+ channels of the BK-type in the mouse brain. *Histochem. Cell Biol.* **125,** 725–741
55. Henry, K. R. (1979) Auditory brainstem volume-conducted responses: origins in the laboratory mouse. *J. Am. Aud. Soc.* **4,** 173–178
56. Galbraith, G., Waschek, J., Armstrong, B., Edmond, J., Lopez, I., Liu, W., and Kurtz, I. (2006) Murine auditory brainstem evoked response: putative two-channel differentiation of peripheral and central neural pathways. *J. Neurosci. Methods* **153,** 214–220
57. Pierce, E. T. (1973) Time of origin of neurons in the brain stem of the mouse. *Prog. Brain Res.* **40,** 53–65
58. Marrs, G. S., and Spirou, G. A. (2012) Embryonic assembly of auditory circuits: spiral ganglion and brainstem. *J. Physiol.* **590,** 2391–2408
59. Tritsch, N. X., Yi, E., Gale, J. E., Glowatzki, E., and Bergles, D. E. (2007) The origin of spontaneous activity in the developing auditory system. *Nature* **450,** 50–55
60. Tritsch, N. X., Rodríguez-Contreras, A., Crins, T. T., Wang, H. C., Borst, J. G., and Bergles, D. E. (2010) Calcium action potentials in hair cells pattern auditory neuron activity before hearing onset. *Nat. Neurosci.* **13,** 1050–1052
61. Hoffpauir, B. K., Kolson, D. R., Mathers, P. H., and Spirou, G. A. (2010) Maturation of synaptic partners: functional phenotype and synaptic organization tuned in synchrony. *J. Physiol.* **588,** 4365–4385
62. Dolmetsch, R. E., Pajvani, U., Fife, K., Spotts, J. M., and Greenberg, M. E. (2001) Signaling to the nucleus by an L-type calcium channel-calmodulin complex through the MAP kinase pathway. *Science* **294,** 333–339
63. Bito, H., and Takemoto-Kimura, S. (2003) Ca(2+)/CREB/CBP-dependent gene regulation: a shared mechanism critical in long-term synaptic plasticity and neuronal survival. *Cell Calcium* **34,** 425–430
64. Sheng, M., Thompson, M. A., and Greenberg, M. E. (1991) CREB: a Ca(2+)-regulated transcription factor phosphorylated by calmodulin-dependent kinases. *Science* **252,** 1427–1430
65. Deisseroth, K., Heist, E. K., and Tsien, R. W. (1998) Translocation of calmodulin to the nucleus supports CREB phosphorylation in hippocampal neurons. *Nature* **392,** 198–202
66. Zirpel, L., Janowiak, M. A., Veltri, C. A., and Parks, T. N. (2000) AMPA receptor-mediated, calcium-dependent CREB phosphorylation in a subpopulation of auditory neurons surviving activity deprivation. *J. Neurosci.* **20,** 6267–6275
67. Zirpel, L., Lippe, W. R., and Rubel, E. W. (1998) Activity-dependent regulation of [Ca2+]*i* in avian cochlear nucleus neurons: roles of protein kinases A and C and relation to cell death. *J. Neurophysiol.* **79,** 2288–2302
68. Schweigreiter, R. (2006) The dual nature of neurotrophins. *Bioessays* **28,** 583–594
69. Hafidi, A. (1999) Distribution of BDNF, NT-3 and NT-4 in the developing auditory brainstem. *Int. J. Dev. Neurosci.* **17,** 285–294
70. Hafidi, A., Moore, T., and Sanes, D. H. (1996) Regional distribution of neurotrophin receptors in the developing auditory brainstem. *J. Comp. Neurol.* **367,** 454–464
71. Yan, Q., and Johnson, E. M. (1988) An immunohistochemical study of the nerve growth factor receptor in developing rats. *J. Neurosci.* **8,** 3481–3498
72. Sasaki, Y., Ohsawa, K., Kanazawa, H., Kohsaka, S., and Imai, Y. (2001) Iba1 is an actin-cross-linking protein in macrophages/microglia. *Biochem. Biophys. Res. Commun.* **286,** 292–297
73. Noailles, A., Fernández-Sanchez, L., Lax, P., and Cuenca, N. (2014) Microglia activation in a model of retinal degeneration and TUDCA neuroprotective effects. *J. Neuroinflammation* **11,** 186

74. Brettschneider, J., Toledo, J. B., Van Deerlin, V. M., Elman, L., McCluskey, L., Lee, V. M., and Trojanowski, J. Q. (2012) Microglial activation correlates with disease progression and upper motor neuron clinical symptoms in amyotrophic lateral sclerosis. *PLoS ONE* **7,** e39216
75. Lv, P., Kim, H. J., Lee, J. H., Sihn, C. R., Fathabad Gharaie, S., Mousavi-Nik, A., Wang, W., Wang, H. G., Gratton, M. A., Doyle, K. J., Zhang, X. D., Chiamvimonvat, N., and Yamoah, E. N. (2014) Genetic, cellular, and functional evidence for Ca2+ inflow through Cav1.2 and Cav1.3 channels in murine spiral ganglion neurons. *J. Neurosci.* **34,** 7383–7393
76. Rubel, E. W., Parks, T. N., and Zirpel, L. (2004) Assembling, connecting and maintaining the cochlear nucleus, in *Plasticity of the Auditory System* (Parks, T. N., Rubel, E. W., Fay, R. R., and Popper, A. N., eds), pp. 9–48, Springer Publishing, New York
77. Maricich, S. M., Xia, A., Mathes, E. L., Wang, V. Y., Oghalai, J. S., Fritzsch, B., and Zoghbi, H. Y. (2009) Atoh1-lineal neurons are required for hearing and for the survival of neurons in the spiral ganglion and brainstem accessory auditory nuclei. *J. Neurosci.* **29,** 11123–11133
78. Mostafapour, S. P., Cochran, S. L., Del Puerto, N. M., and Rubel, E. W. (2000) Patterns of cell death in mouse anteroventral cochlear nucleus neurons after unilateral cochlea removal. *J. Comp. Neurol.* **426,** 561–571
79. Levi-Montalcini, R. (1949) The development to the acoustico-vestibular centers in the chick embryo in the absence of the afferent root fibers and of descending fiber tracts. *J. Comp. Neurol.* **91,** 209–241
80. Lachica, E. A., Rübsamen, R., Zirpel, L., and Rubel, E. W. (1995) Glutamatergic inhibition of voltage-operated calcium channels in the avian cochlear nucleus. *J. Neurosci.* **15,** 1724–1734
81. Sanes, D. H., and Friauf, E. (2000) Development and influence of inhibition in the lateral superior olivary nucleus. *Hear. Res.* **147,** 46–58
82. Lipton, S. A., and Kater, S. B. (1989) Neurotransmitter regulation of neuronal outgrowth, plasticity and survival. *Trends Neurosci.* **12,** 265–270
83. Berridge, M. J., Bootman, M. D., and Lipp, P. (1998) Calcium: a life and death signal. *Nature* **395,** 645–648
84. Friauf, E. (1994) Distribution of calcium-binding protein calbindin-D28k in the auditory system of adult and developing rats. *J. Comp. Neurol.* **349,** 193–211
85. Lohmann, C., and Friauf, E. (1996) Distribution of the calcium-binding proteins parvalbumin and calretinin in the auditory brainstem of adult and developing rats. *J. Comp. Neurol.* **367,** 90–109
86. Caicedo, A., d'Aldin, C., Eybalin, M., and Puel, J. L. (1997) Temporary sensory deprivation changes calcium-binding proteins levels in the auditory brainstem. *J. Comp. Neurol.* **378,** 1–15
87. Zheng, F., Zhou, X., Luo, Y., Xiao, H., Wayman, G., and Wang, H. (2011) Regulation of brain-derived neurotrophic factor exon IV transcription through calcium responsive elements in cortical neurons. *PLoS ONE* **6,** e28441
88. Tabuchi, A., Nakaoka, R., Amano, K., Yukimine, M., Andoh, T., Kuraishi, Y., and Tsuda, M. (2000) Differential activation of brain-derived neurotrophic factor gene promoters I and III by Ca2+ signals evoked via L-type voltage-dependent and *N*-methyl-D-aspartate receptor Ca2+ channels. *J. Biol. Chem.* **275,** 17269–17275
89. Tao, X., Finkbeiner, S., Arnold, D. B., Shaywitz, A. J., and Greenberg, M. E. (1998) Ca2+ influx regulates BDNF transcription by a CREB family transcription factor-dependent mechanism. *Neuron* **20,** 709–726
90. Paul, C. E., Vereker, E., Dickson, K. M., and Barker, P. A. (2004) A pro-apoptotic fragment of the p75 neurotrophin receptor is expressed in p75NTRExonIV null mice. *J. Neurosci.* **24,** 1917–1923
91. Chonko, K. T., Jahan, I., Stone, J., Wright, M. C., Fujiyama, T., Hoshino, M., Fritzsch, B., and Maricich, S. M. (2013) Atoh1 directs hair cell differentiation and survival in the late embryonic mouse inner ear. *Dev. Biol.* **381,** 401–410
92. Hoffpauir, B. K., Marrs, G. S., Mathers, P. H., and Spirou, G. A. (2009) Does the brain connect before the periphery can direct?: A comparison of three sensory systems in mice. *Brain Res.* **1277,** 115–129
93. Balakrishnan, V., Becker, M., Löhrke, S., Nothwang, H. G., Güresir, E., and Friauf, E. (2003) Expression and function of chloride transporters during development of inhibitory neurotransmission in the auditory brainstem. *J. Neurosci.* **23,** 4134–4145
94. Blaesse, P., Guillemin, I., Schindler, J., Schweizer, M., Delpire, E., Khiroug, L., Friauf, E., and Nothwang, H. G. (2006) Oligomerization of KCC2 correlates with development of inhibitory neurotransmission. *J. Neurosci.* **26,** 10407–10419
95. Löhrke, S., Srinivasan, G., Oberhofer, M., Doncheva, E., and Friauf, E. (2005) Shift from depolarizing to hyperpolarizing glycine action occurs at different perinatal ages in superior olivary complex nuclei. *Eur. J. Neurosci.* **22,** 2708–2722
96. Kullmann, P. H., Ene, F. A., and Kandler, K. (2002) Glycinergic and GABAergic calcium responses in the developing lateral superior olive. *Eur. J. Neurosci.* **15,** 1093–1104
97. Tierney, T. S., Russell, F. A., and Moore, D. R. (1997) Susceptibility of developing cochlear nucleus neurons to deafferentation-induced death abruptly ends just before the onset of hearing. *J. Comp. Neurol.* **378,** 295–306
98. Bean, B. P. (2007) The action potential in mammalian central neurons. *Nat. Rev. Neurosci.* **8,** 451–465
99. Koschak, A., Reimer, D., Huber, I., Grabner, M., Glossmann, H., Engel, J., and Striessnig, J. (2001) α1D (Cav1.3) subunits can form L-type Ca2+ channels activating at negative voltages. *J. Biol. Chem.* **276,** 22100–22106
100. Lipscombe, D., Helton, T. D., and Xu, W. (2004) L-type calcium channels: the low down. *J. Neurophysiol.* **92,** 2633–2641
101. Willaredt, M. A., Ebbers, L., and Nothwang, H. G. (2014) Central auditory function of deafness genes. *Hear. Res.* **312,** 9–20
102. Schneggenburger, R., Meyer, A. C., and Neher, E. (1999) Released fraction and total size of a pool of immediately available transmitter quanta at a calyx synapse. *Neuron* **23,** 399–409

Neurobiology:

L-type Calcium Channel $Ca_V1.2$ Is Required for Maintenance of Auditory Brainstem Nuclei

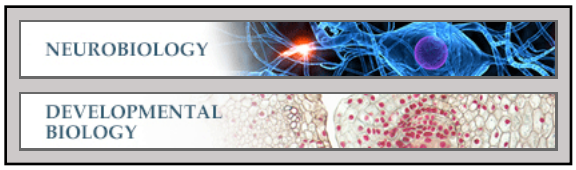

Lena Ebbers, Somisetty V. Satheesh, Katrin Janz, Lukas Rüttiger, Maren Blosa, Franz Hofmann, Markus Morawski, Désirée Griesemer, Marlies Knipper, Eckhard Friauf and Hans Gerd Nothwang

J. Biol. Chem. 2015, 290:23692-23710.
doi: 10.1074/jbc.M115.672675 originally published online August 4, 2015
